Report by IOC/UNESCO TOWS-WG
Team on Atypical Tsunami Sources
(Version 15th February 2022)

Introduction – Objective

After the recent destructive tsunamis due to landslides, volcanic eruptions and earthquakes in Indonesia in 2018 and in Greenland in 2017, the IOC/UNESCO Working Group on Tsunamis and Other hazards related to sea level Warning and mitigations Systems (TOWS-WG) identified the need to provide IOC Member States with a report that includes information and knowledge about the specific tsunami warning systems required for such atypical tsunami events. A specific team was accordingly established under the TOWS-WG Task Team on Tsunami Watch Operations. The mandate of the team is to investigate these events, the current state of the art related to monitoring and warning for such events, and provide guidance and recommendations to the Member States.

In this report, a typical tsunami means a tsunami caused by a large megathrust earthquake source, i.e., a low angle reverse fault type earthquake (so called a thrust type of earthquake) that occurs at subduction zonesaround the world. Thus, an atypical tsunami is defined as a tsunami from other sources besides such thrust earthquakes occurring on the subduction interfaces.

Atypical tsunamis can be further divided into two categories, namely seismic sources and non-seismic sources. Sources of atypical tsunami can also be further classified. In seismic sources of atypical tsunamis, there are crustal faults including normal fault type earthquakes (e.g. Loyalty Islands earthquakes in Nov. 2017), strike slip fault type earthquakes (e.g. Cayman Islands earthquake on 28 Jan., 2020), events occurring in splay faults, as well as thurst type events occurring outside (and ofter far from) subducton interfaces (e.g. 2003 M6.8 Boumerdes earthquakes in Algeria). In non-seismic sources of atypical tsunamis, there are volcanic sources such as underwater explosions, pyroclastic flows, large scale collapses and so on, as well as submarine landslides and tsunamis triggered by meteorological perturbations (meteotsunamis).

Table of contents

1. Non-Megathrust Tsunami Earthquakes

A number of destructive tsunamis have been historically associated with megathrust systems, with the most recent examples being the significant earthquakes and associated tsunamis of the 2004 Indian Ocean Tsunami (IOT 2004) and the 2011 Tohoku Earthquake and Tsunami. However, destructive tsunamis have also been associated with non-mega thrust systems. For example, in the NE Caribbean the 1867 Anegada Passage event generated a significant tsunami of ~7-9m height observed at St Croix (Zahibo et al, 2003) and the 1918 Mona Passage event generated a tsunami of >6m height observed in North-western Porto Rico (Reid & Taber, 1919). The latter of these two examples may have included contributions to the tsunami size from a submarine landslide triggered by the earthquake (Lopez-Venegas et al, 2008). Additionally, non-mega thrust tsunamis exist in the historical tsunami catalogues of the Mediterranean (Maramai et al, 2014), such as the 1908 Mw7.1 Messina Straits earthquake with wave heights > 10m making a significant contribution to the overall death toll (Guidoboni et al., 2019), again with the possible contribution from a seismically induced submarine landslide (e.g., Favalli et al., 2009). More recently, the 2003 Mw 6.8 Zemmouri-Boumerdes tsunami recorded a maximum wave height of ~2m in the Balearic Islands (Alasset et al, 2006). While this event had a reverse (thrust) focal mechanism, the earthquake was not located along a traditional subduction zone, but rather the complex zone of convergent and lateral motion associated with the collision of the Eurasian and African plates (Hamadache et al, 2004; Santos et al, 2015; Alasset et al, 2006). Similarly, the 2017 Kos-Bodrum M6.6 or the recent 2020 Izmir-Samos M7.0 normal fault earthquakes generated significant damaging tsunamis (Dogan et al., 2019; Yalciner et al., 2020). Notably, examples in the Caribbean and the Mediterranean occur along complex oblique plate boundaries indicating that such boundaries have to be included in tsunami modeling. While deciphering these complex boundaries is a problem akin to unraveling a Gordian knot, a smart management of this type of events into regional and local tsunami hazard and risk analyses should be a priority, at least for such regions characterized by complex tectonic settings. In the following, we first introduce a statistical analysis of recent tsunamis to highlight the potential contribution of non-megathrust earthquakes into the total tsunami threat (section 1.2), then we review some recent examples of the handling of such events in terms of hazard quantification and warning management.

Notably the earthquake crisis that occurred in Loyalties islands seismic zone, with 5 normal fault quakes of magnitude 6.3 to 7.0, generated tsunamis recorded by tide gauges on the coast of New Caledonia and Loyalties islands. Such normal fault quakes had an important larger tsunami potential, even larger than the typical thrust quakes, because the much higher dip (35 – 45°) likely induced a larger vertical motion of the sea floor, compared to similar thrust fault ruptures. Significant tsunamis are also however possible for non-subduction thrust events (e.g., 2003 M6.8 Boumerdes earthquakes), or even large strike-slip events (e.g., 2019 M7.5 Palu earthquake), generating significant local tsunamis that may be possibly enanced by local small seismically induced landslides (Beherens et al, 2021). Consequently, all potential focal mechanisms should be in principle considered as potential tsunami generators, with the main focus to normal and thrust events.

1.1 Prevalence of non-thrust mechanism tsunamis

Destructive tsunamis are short fuse events. Albeit relatrively rare, they are extremely dangerous and allow little to no time for warning. They are difficult to prepare for, as they occur relatively infrequently, but can have severe consequences Non-thrust earthquakes located close to coastlines or inland that generate destructive tsunamis may provide for an even shorter fuse event. To explore this a database combining tsunamis in the NOAA Historical Tsunami Catalog (NGDC, 2017) generated by an earthquake with the focal mechanisms available in the Harvard Global CMT Catalog (Dziewonski et al, 1981; Ekstrom et al,

2012). For the analysis, each event was required to have an available CMT solution, as well as a defined Maximum Water Height in the Tsunami catalogue. This provides a database of 345 earthquakes associated with tsunamis with a measured maximum wave height between January 1976 and January 2020. Note the Caribbean examples described above would be considered non-thrust events in this analysis, whereas some of the Mediterranean examples (the Zemmouri-Boumerdes event) would be considered a thrust event based on its focal mechanism (reverse faults), despite not being located along a subduction zone. Nevertheless, such reverse faults with much larger dip (> 35°) in comparison of thrust faults (< 15°) generate sea floor deformation 2-4 times larger than typical thrust faults.

To evaluate the impact of non-subduction zone earthquakes a map containing the data in conjunction with the Slab2.0 model of Hayes, (2018) has been produced (Figure 1). The global map indicates that most of the tsunamigenic events in the dataset are predominantly associated with active subduction. However, some tsunamigenic events do occur in regions well removed from these active margins. Some of the outliers are sourced in regions of active ocean island volcanism, such as Hawaii in the central Pacific. Where as other events are associated with incipient or diffuse tectonic features such as possible thrust wrench faulting off the coasts of Iberia (Rosas et al, 2016), along ocean ridges, or along structures such as the 90ºE ridge which may be a diffuse plate boundary cutting the Indo- Australian Plate in two (Royer and Gordon, 1997). Nonetheless, Figure 1 demonstrates that these non- megathrust earthquakes are likely rarer and therefore for emergency management purposes are even harder to prepare for. However, in areas with complex tectonic settings like the Caribbean, the Mediterranean or within the Indonesian archipelago, non megathrust events might represent the majority of the reported events.

To further explore the impact of these non-thrust events by separating thrust events into mega-thrust and non-mega thrust events would require local expertise for each region. The data presented here helps further explore by using the general focal mechanism type. For ease of analysis the data is sorted into general types based upon the variable Rake1 recorded in the CMT Catalog, for details see Table 1.

While this same sorting was also performed for CMT Catalog Rake2 with analogous results, here the document will concentrate on commenting primarily on the results from Rake1. Figure 2 shows the distribution of rake and the associated recorded wave height in meters. The plot does not include 5 events with measured wave height >25m and rake between 80º and 110º (thrust events). While the plurality of events occur within the thrust regime, the plot demonstrates that significant tsunamis with wave heights >1m also occur in normal and oblique faulting regimes.

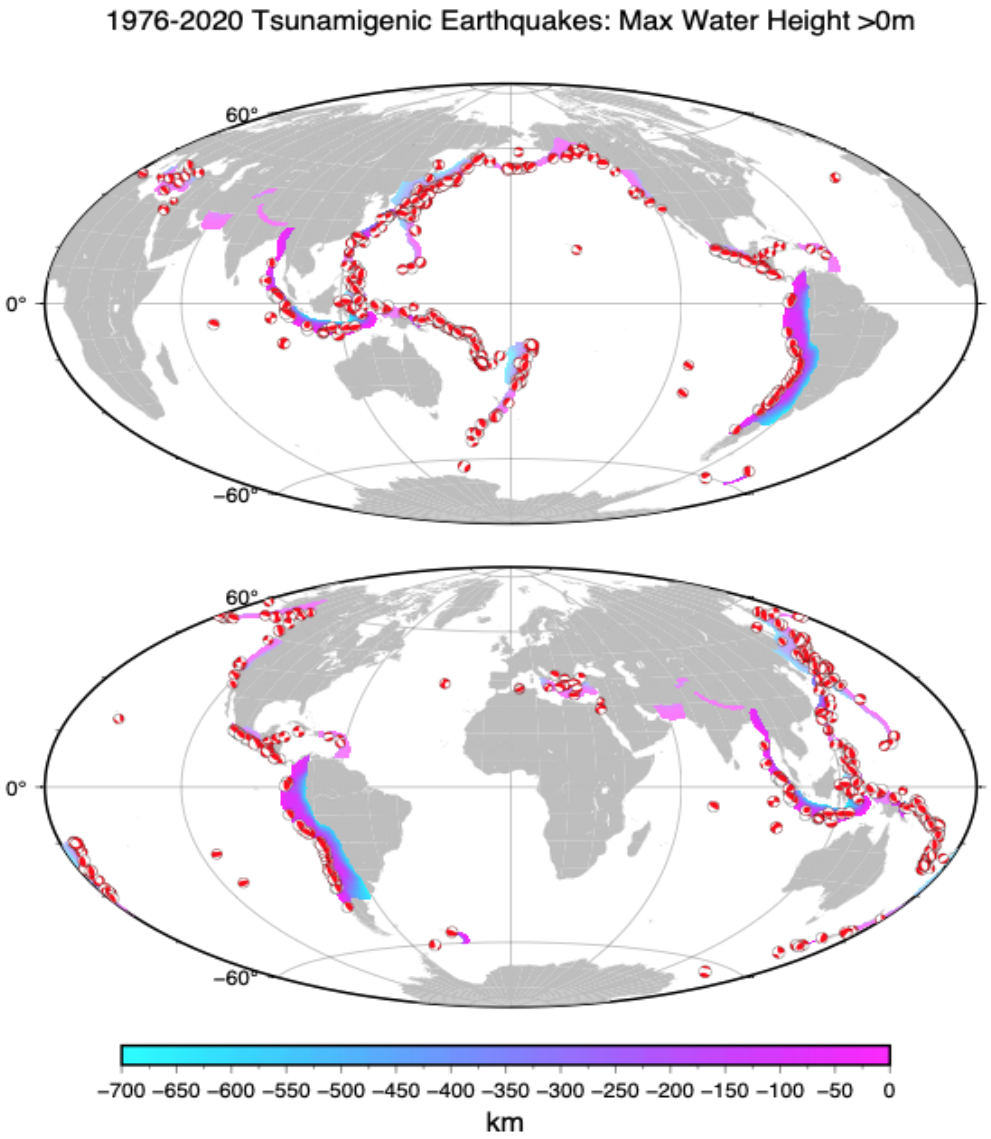

Figure 1: *Map of the Earthquakes tsunami sources (1976--Jan 2020) that have a recorded CMT Focal Mechanism and a recorded water height in the NOAA Historical Tsunami Catalog. Note that these events predominantly occur along subduction zones, but this is not always the case.*

Earthquake Type	Rake(R1) Range (in º)
Reverse	70<R1<=110
Normal	-160<R1<-110
Oblique Reverse-Strike Slip	Left lateral: 20<R1<=70 Right Lateral: 110<R1<=160
Oblique Normal -Strike-Slip	Left lateral: -70<R1<-20 Right Lateral: -160<R1<-110
Strike-Slip	Left lateral: -20<=R1<=20 Right Lateral: R1<=-160 or R1>=160

Table 1: Rake ranges applied to classify the dataset for analysis.

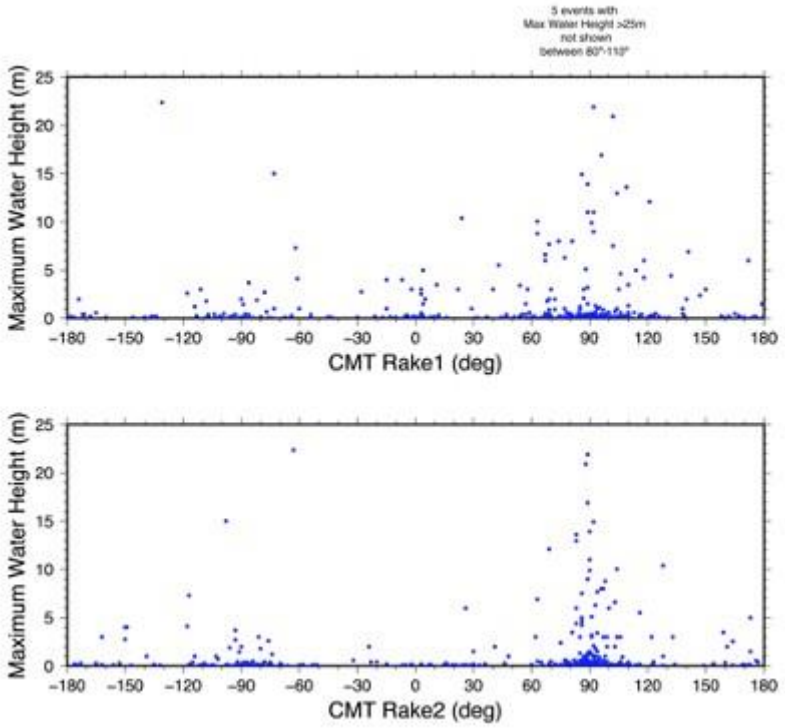

Figure 2: Distribution of maximum wave height with respect to the Harvard CMT rake. Note that significant tsunamis have occurred across the rake range. The 5 largest events, with maximum wave heights >25m and clear origin being megathrust, are not included in the plot.

Sorting further, using Rake1 and the maximum water height one can determine the percentages of events creating potentially damaging tsunami waves based on the historical database. The results of the sorting by both wave height as well as rake permit an estimation of the occurrence rate of non- thrust tsunamis. The numerical data from the analysis is included in Table 2. The analysis yields that for all tsunamigenic events approximately 64% are associated with reverse or oblique reverse motions, whereas the remaining 36% is split evenly between normal/oblique normal and strike-slip motions. In contrast for events in which the maximum water height is >1m the analysis yields that ~70% are associated with reverse or oblique reverse motions, 14% are associated with strike-slip classed events, and 16% with normal/oblique normal events. This demonstrates that rarer non-thrust events can and do generate significant tsunamis.

Earthquake Type	Number of Tsunamis	Max Water Height <0.3m	Max Water Height >=0.3m & <1m	Max Water Height >1m
Reverse	141	78	30	33
Normal	35	19	9	7
Oblique Reverse-Strike Slip	81	40	15	26
Oblique Normal - Strike-Slip	27	18	2	7
Strike-Slip	61	41	8	12

Table 2: *Distribution of tsunamis classed by wave height. Note most highly destructive tsunamis occur in the Reverse or Oblique Reverse (thrust) regime, but rare impactful tsunamis with water heights >1m do occur in other regimes.*

1.2 Inclusion of non-thrust mechanism tsunamis into tsunami hazard and warning: examples from the NEAM region

As discussed in Section 1.1, in complex tectonic settings and small basins such as the Mediterranean region, the Caribbean, or around the Indonesian archipelago, non-megathrust tsunamis sources may represent the majority of potential tsunamigenic sources. Taking for example the Mediterranean, tsunami catalogues (Maramai et al., 2014) and hazard disaggregation results (Selva et al., 2016; Basili et al., 2018, 2019, 2020) show that the contribution to the total tsunami hazard of crustal sources is also significant along the coasts exposed to subduction zone generated tsunamis.

The inclusion of these sources in tsunami forecasts (both PTHA and forecasts for TWSs) is very challenging. Tsunami forecasts are typically based on the definition of a set of individual sources covering the whole natural variability, the quantification of the probability of occurrence of each source, and the simulation of the tsunami generation and propagation for each individual source, usually adopting non-linear models in shallow water approximation (Grezio et al., 2017; Selva et al. 2021a). However, non-subduction seismicity can be spread over large source areas and includes a broad variety of source mechanisms. This implies a very large source variability that challenges their representation in tsunami forecasts. As a consequence, the integration of such sources into PTHA and TWS depends on the development of specific computational and methodological strategies (e.g., Molinari et al., 2016; Selva et al., 2016, 2019; Løvholt et al., 2019,2020) and it is very often neglected. Selva et al. (2021a) recently discussed the ongoing effort to manage such types of sources for the Italian coasts in the central Mediterranean, ranging from available hazard quantifications to the existing efforts to include such sources into tsunami warning.

The NEAM region (North-East Atlantic, the Mediterranean and connected seas) has its own recent S-PTHA model, called NEAMTHM18 (NEAM Tsunami Hazard Model; Basili et al., 2018, 2019, 2021; http://www.tsumaps-neam.eu/). NEAMTHM18 was produced by the TSUMAPS-NEAM project (2016-2018), which was co-funded by the Directorate-General European Civil Protection and Humanitarian Aid Operations (DG-ECHO). The seismic sources considered by NEAMTHM18 are not limited to the subduction zones, as the crustal seismicity is also taken into account (Selva et al., 2016; Basili et al., 2021), including seismicity in the subduction zone not located on the slab (e.g., in the accretionary wedge and continental crust, including splay faults, and outer-rise earthquakes in the oceanic crust), and the remaining interplate seismicity. To optimally deal with this heterogeneous degree of knowledge of diffuse seismicity, while maximizing the use of all the available information, the seismicity is subdivided into two categories: a) Background seismicity, used for treating crustal earthquakes; and b) Predominant seismicity, used for dealing mainly with subduction-related events. This approach to seismicity types in probabilistic calculations was firstly introduced for S-PTHA (Selva et al., 2016), in line with other approaches introducing faults into PSHA studies (Field et al., 2014, 2017; Woessner et al., 2015).

NEAMTHM18 was adopted as a starting point for the Italian national coastal planning initiative for seismically generated tsunamis (Dipartimento della Protezione Civile, 2018; Selva et al. 2021a Dipartimento della Protezione Civile, 2018), which chose as the design tsunami intensity for tsunami warning the Maximum Inundation Height corresponding to the 2500 years average return period on the 84th percentile curve of the epistemic uncertainty. To account for the limited spatial resolution and the relatively coarse sampling of the source parameter space of NEAMTHM18, several safety factors have been defined to define the design run-up values (Dipartimento della Protezione Civile, 2018; Tonini et al. 2021). To evaluate the inundation zones from maximum run-up values, dissipation limiting the inundation distance is included that adopts the empirical relationships very similar to those proposed for New Zealand (Leonard et al., 2008; New Zealand and Ministry of Civil Defense & Emergency Management, 2008, 2016; Fraser & Power, 2013). A project aiming to refine the hazard model limiting the target area to the Italian coasts is ongoing (Selva et al., 2021a).

Non-megathrust tsunamis need also be considered in tsunami warnings. To deal with all potential sources in relatively short time-scales (required in small basins), all tsunami warning centres of NEAM are at present using Decision Matrices (DMs). The main advantage of using DMs is the fact that forecasts and alert levels may be timely produced as soon as basic information about the source earthquake is available, independently of the type of seismic source. DMs require only location, depth and magnitude, that is the information typically available and sufficiently stable just a few minutes after the origin time where network is densed (Bernardi et al., 2015). This is not the case for very large earthquake with duration of larger than several minutes (Chile 1960, Sumatra 2004…). However, DMs overlook the complex propagation pattern that is mainly controlled by source geometry and dynamics, as well as by bathymetric features. Despite the conservativeness adopted in their definition, DMs may inevitably lead to both under- and over-estimation, eventually causing missed alarms at specific locations, such as where energy focusing may occur. However, to account for wave propagation is challenging, since it would require a high number of tsunami simulations to consider the very vast variability of the potential sources.

To overcome these problems, a new probabilistic method coined “Probabilistic Tsunami Forecasting (PTF)” is being developed by the NEAMTWS TSP CAT-INGV (Selva et al., 2019,2021b; Løvholt et al., 2019). The PTF is based on the propagation of the uncertainty from the source parameters, as estimated in near real-time from the monitoring room in the warning centre, to the potential impact zone, through pre- calculated tsunami simulations (**Figure** 3). The method allows updating the input data through time, as new information about the seismic source and/or the propagating tsunami is available. The PTF provides as output the probability distribution of the tsunami inundation height at predefined target points. These results can be automatically connected to alert levels. For example, if we define a reference interval of tsunami intensities for each alert level, the PTF would indicate the probability of the different intervals.

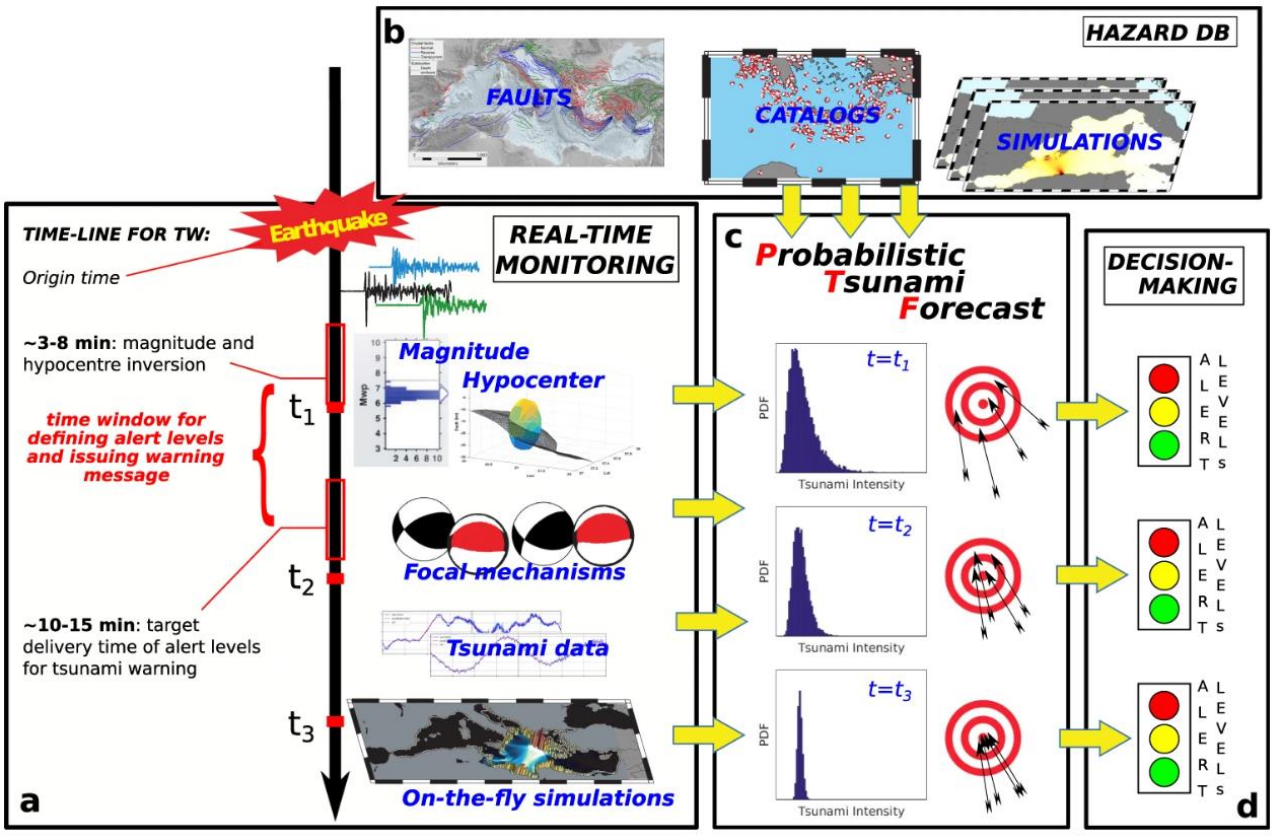

***Figure 3**: Workflow of Probabilistic Tsunami Forecasting (from Selva et al. 2021b). Real-time data (panel a) are integrated with long-term information (panel b) to provide forecasts (panel c) at different times. Based on rules defined in advance by decision-makers, probabilistic forecasts can be transformed into alert levels (panel d), accounting for the uncertainty existing at the time of the estimation.*

The PTF evaluation is based on a pre-computed database derived from the regional hazard model NEAMTHM18, therefore it includes, as discussed above, both subduction and crustal seismicity. This allows also a significant reduction of computational times (< 2 minutes in Selva et al. 2021b, with a non optimized Matlab code, available at https://github.com/INGV/matPTF). Given the requirement of very rapid assessment of the PTF within a relatively small area like the Mediterranean, the reference implementation of the method to deal with near-field tsunamis (with warnings delivered within 10' from the earthquake occurrence) is based on the evaluation of the uncertainty on magnitude and epicenter from the location algorithm (in the case of CAT-INGV, Early- Est; Bernardi et al., 2015 and references therein). On the contrary, uncertainty about the focal mechanism (strike, dip, rake) is typically delivered too late to be included. To compensate for this lack of information, estimations derived from long-term hazard quantifications can be used, adopting the results of NEAMTHM18, in which the long-term probability distribution of potential source mechanisms is set based on local geological (e.g., mapped faults) and historical (e.g., hypothesized earthquake focal mechanisms) information. In the Mediterranean region, this is particularly important since it allows dealing with crustal seismicity, whose kinematics are generally less constrained than subduction seismicity. Selva et al. (2021b) discuss in more details this methodology for a large range of magnitudes and earthquake types, from the great 2010 M8.8 Maule (Chile), to the well-studied 2003 M6.8 Zemmouri-Boumerdes (Algeria) tsunamis, to all moderate magnitudes (in the range 6 to 7) events that have occurred in the Mediterranean in recent times.

Remark –draft preliminary recommendation: Globally, all seismic zones and all potentially tsunamigenic faults should be considered by TSPs, not only subduction interfaces. Examples of such

faults are the normal faults in the NEAM region that moved recently in 2017 and in 2020, and those located in Loyalties islands regions and other regions over subduction zones. This is the major challenge because not all potential active faults have been identified and large uncertainty typically exists in their identification.

One recommendation is to increase the efforts in studying this type of seismic zones, and to use the current Global CMT database (from 1976), or more recent regional versions (RCMT, like the one available for the Mediterranean, REF) to identify those areas that already produced earthquakes that could generate tsunamis.

The problem of the Figure based on recorded tsunamis (Figure 1) is the incompleteness of the sea level data. Until 2004-2012 in the Pacific, Indian Ocean, Caribbean and Mediterranean region etc, only a few tide gauges able to record tsunami waves were implemented or the data available. Sstill recently several events have occurred in Greece from 2015 to 2020 that were recorded well by only a few tide gauges. We could conclude that probably most of the events that occurred in the past of magnitude 6 to 7 could have generated small local tsunamis that were never recorded or observed and thus are missing in all catalogues and databases.

One suggestion to improve the systems could be for all shallow (< 30 km) submarine and coastal normal or thurst faults that may generate quakes of magnitude larger than 6.0 should be taken into account in the data base of the TSsP. Similar suggestions could be made for mix reverse-strike or normal- strike earthquakes for slightly larger magnitudes (e.g. > 6.3 – 6.5). Considering the potential for multiple source mechanisms in most of these seismic zones and the uncertainty in real-time inversion, efforts to manage existing uncertainty may facilitate their effective inclusions in TSP operations.

2. OTHER GEOPHYSICAL SOURCES (LANDSLIDES, VOLCANOES,…)

Three countries have implemented tsunami volcano monitoring and warning systems:

- Japan (since XXX), Italy (Stromboli - 2003), Indonesia (Anak Krakatau - 2019).

No tsunami monitoring or warning systems exist for landslides or submarine landslides not potentially generated by volcanoes.

2.1 MONITORING

2.1.1 Italy - Stromboli

Stromboli Island (Italy) is an active volcano characterized by persistent Strombolian activity, with persistent low energy explosion activity and episodic larger explosions and lava flows (Figure 4). Flank eruptions, paroxysmal explosions, or deformation during effusive phases often contribute to generating large mass failures along the Sciara del Fuoco (SdF), which is the most unstable sector of the volcanic edifice. Landslides, and therefore tsunamis, triggered by paroxysms usually occur a few minutes after the explosion. These explosions typically do not show any kind of precursors in the short-term (hours or days), but in the very short-term (minutes) they show changes in deformation of the edifice (Ripepe and Harris, 2005; Marchetti et al., 2009; Pistolesi et al., 2011; Di Traglia et al., 2014; Valade et al., 2016; Giudicepietro et al., 2020; Ripepe et al., 2021). Flank instability occurs often during effusive phases, during which ground deformation is crucial to identify early stages of magma intrusions and instability scenarios (Ripepe et al., 2009; 2015; Marchetti et al., 2009; Di Traglia et al., 2014; Valade et al., 2016).

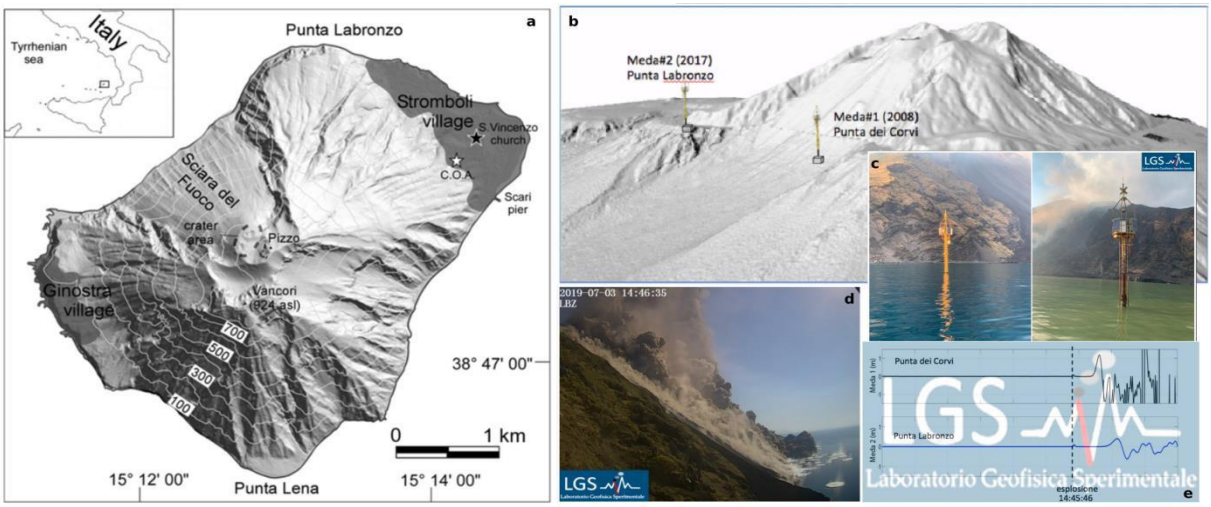

Figure 4: *(a) DEM of Stromboli Island with main geographic features, from Bertolaso et al. (2009). White zone: active vents area; white star: location of the Civil Protection Advanced Operational Center (COA). (b) Elastic beacons (MEDA) used for monitoring tsunamis at Stromboli and the 3 July 2019 tsunami: showing the position and anchorage of the MEDA. (c) TheMEDA just after the 03/07/2019 pyroclastic flow (photos courtesy of the Italian Coast Guard). (d) Snapshot of the 03/07/2019 pyroclastic flow. (e) Tsunami signals recorded at the MEDA during the 03/07/2019 event. Pictures and Figures adapted from http://lgs.geo.unifi.it/index.php/blog/tsunami-registrato-stromboli-3-luglio-2019 and Lacanna and Ripepe (2020).*

The monitoring system at Stromboli is based on two main components (Dipartimento della Protezione Civile and Regione Sicilia, 2015; Lacanna and Ripepe, 2020a; Selva et al. 2021a):

a) Multi-parametric network with several monitoring networks (e.g., seismo-acoustic stations, thermal cameras, tiltmeters, etc.) designed to identify anomalies to observe or forecast transitions between different eruptive phases in the volcanic activity.

b) Two elastic beacons (MEDA) located offshore (approximately 300 m) to the sides of SdF (Figure 3(c)) have been designed to detect tsunami waves in real-time, transmitting data to the civil protection's Advanced Operational Center (COA), located in Stromboli.

Tsunami detection is based on the elastic beacons. The two beacons (MEDA) are semi-rigid structures made of a 30 m long metallic pole, anchored to the sea floor with a 20 Tons deadweight (Figure 3). The MEDA reaches 8 m of height above the sea surface and is equipped with multiple sensors, as well as power supply and radio transmission systems (Lacanna and Ripepe, 2020). Sensors include hydrostatic pressure (sampled at 4 Hz), temperature (sampled at 1 Hz), hydroacoustic noise (sampled at 40 Hz), GPS and 2 tiltmeters (sampled 4 Hz). Thery provide measures of interest for tsunami detection and measures to monitor the operability and the performance of the station. The characteristics of the two beacons are reported in Table 3. Three alternative networks send data to the COA, guaranteeing redundancy of data transmission from the stations.

TSUNAMI DETECTION SYSTEM TECHNICAL DETAILS	
Type	Elastic beacon (MEDA)
Quantity	2 (PDC and PLB)
Installation date	2008 and 2017
Location	PDC: 260 m off Punta dei Corvi PLB: 350 m off Punta Labronzo
Length (excluding anti-torsion steel cable)	30 m
Deadweight	20 Tons
Height (a.s.l.)	8 m
Tsunami detection sensors	2 pressure sensors (125 Hz) on board of each elastic beacon located at 14 meters and 50 meters depth
Data transmission	Wi-Fi 5Ghz Radio

Table 3: Technical details of the tsunami detection system installed at Stromboli.

2.1.2 Indonesia – Anak Krakatau

The tsunami caused by the activities of Anak Krakatau on 22 December 2018 can be considered as the first tsunami caused by volcanic avalanches since the establishment of BMKG (*Badan Meteorologi, Klimatologi, dan Geofisica* – Institute of Meteorology, Climatology, and Geophysic) in the 1950s, with the notable exception of the Iliwerung landslide in 1979 (539 people killed). This created great difficulties, as the tsunami warning system was not designed for rare atypical tsunamis. In Indonesia, a tsunami early warning system (InaTEWS) has been in operation since 2008 following the IOT 2004. It is able to detect and warn for tsunamis triggered by earthquakes. BMKG conveys the warning information via SMS, TV broadcasts, radio, website, and BMKG official social media. However, this tsunami warning scenario is only prepared to anticipate tsunamis caused by tectonic activity, not by volcanic activity or landslides.

It is indeed difficult to provide a tsunami warning caused by this source, apart from the fact that the frequency is very rare, there are two agencies in Indonesia who are authorized to rapidly provide the related information. BMKG with a tsunami early warning system and *Pusat Vulcanologi dan Mitigasi Bencana Geologi* (PVMBG- Center of Volcanology and Geological Hazard Mitigation) with a volcano early warning system. Operational communication between the two agencies was not well established for the rare 2018 Krakatau tsunami. So, the first thing that has been done by these two agencies is improving communication, sharing data and information.

Now coordinated monitoring of the volcanic activity of Anak Krakatau is carried out intensively by the two authorized agencies. PVMBG is authorized to monitor volcanic activity using visual and instrumental methods with seismic, deformation, infrasound, and geochemical methods. BMKG is authorised to monitor tectonic activity and issue tsunami warnings. The visual volcanic activity method is carried out by the Anak Krakatau volcano observation station in Pasauran, Banten province, and also the Kalianda station, Lampung province. These observation stations are equipped with thermal and visual cameras (CCTV) to observe the Krakatau volcano continuously for 24 hours. Five seismic instruments have been installed on Anak Krakatau volcano and also on Sertung Island for monitoring volcanic earthquakes.

To monitor tectonic activity around the Sunda Strait, BMKG has also built a denser seismograph network. As the InaTEWS is built to capture earthquakes that can cause tsunamis due to tectonic

earthquakes with a large magnitude, these new efforts are aimed at capturing earthquakes by local tectonic activity and the volcanic activity of Anak Krakatau. BMKG has built an automated system called InaSEIS for 24/7 monitoring of seismic activity around Krakatau with 6 nearby sensors which can provide real-time alerts of seismic local activities around Krakatau (Figure 5).

Figure 5: Anak Krakatau monitoring network

For tsunami warnings, apart from utilizing the tide gauge that existed before the 2018 Anak Krakatoa tsunami, a new sea-level monitoring network has been installed. Three agencies that are directly involved in InaTEWS operations, namely BMKG, *Badan Informasi Geospasial (*BIG – Institute of Geospatial Information), and *Badan Pengkajian dan Penerapan Teknologi (*BPPT - Agency for the Assessment and Application of Technology), coordinate efforts to monitor and provide tsunami warnings to the community. BIG donated 6 tide gauges to monitor the sea level of the Sunda Strait. BMKG utilises a maritime automatic weather station network in the form of 8 water level monitoring locations (with radar, float or pressure sensor)(Figure 4). BPPT has installed a pressure gauge buoy (OBPG) in the Anak Krakatau volcano complex in the form of a cable-based transfer system. In addition, two Inexpensive Devices for Sea Level Monitoring (IDSLs), donated by the Joint Research Center (JRC), in collaboration with the Indonesian Tsunami Society, the Marine Research Center of the Ministry of Marine Affairs and Fisheries and BMKG, are integrated into the overall system for sea-level monitoring, data transfer, and warning alert (Figure 6).

Finally, for a tsunami warning, BMKG has tested the WERA radar system to monitor the height and movement of sea waves around the Sunda Strait. By using the height frequency radar method, which is capable of transmitting up to a distance of 200 km, it is hoped that it will be able to detect early tsunami wave activity (Figure 7).

Walter et. al. (2019) showed that seismic waves generated by the Anak landslide in 2018 were observed and identified. They suggested there is potential for practical application in tsunami warning. So, one recommendation would be to implement a dense network of seismometers in all seismic zones (at least every 50 km along the coastline) close to “active” coastal volcanoes (see list in the ANNEX), as well as on the islands located close and in front of seismic zones to detect the T-

Phase generated by submarine landslides. Methods should be developed for identification and characterisations of landslides, such as volume direction of the landslide. Finally, methods should be developed for the estimation of the size of the generated tsunamis for practical use in tsunami warning.

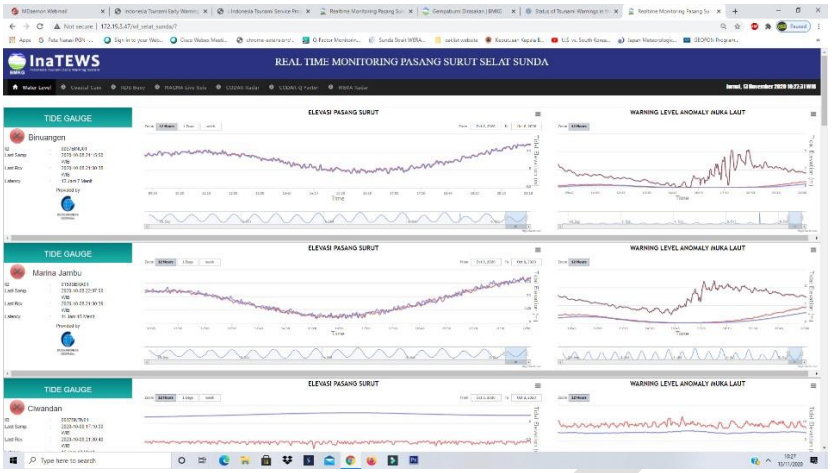

Figure 6: INATEWS sea level monitoring

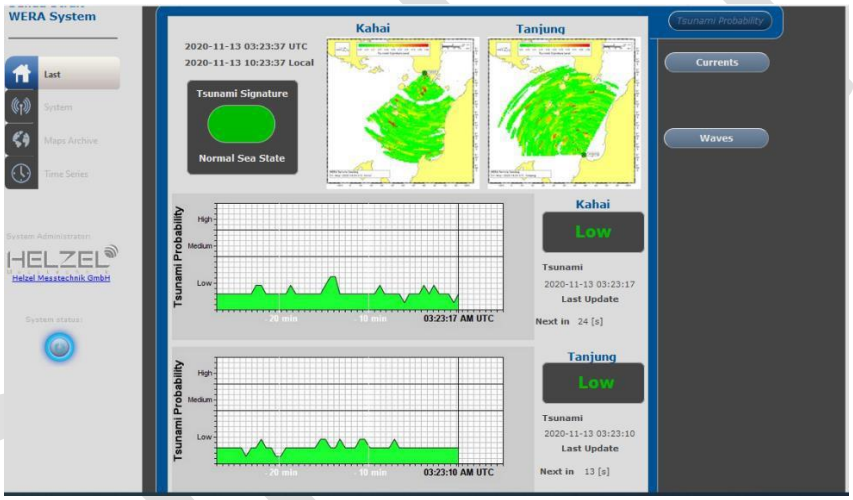

Figure 7: WERA Radar monitoring

2.1.3 Japan – numerous active volcanoes

Seismic monitoring network in Japan (JMA and other organizations)

The Japan Meteorological Agency (JMA) gathers data from its own seismometers installed at approximately 300 locations nationwide, as well as seismometers of the National Research Institute for Earth Science and Disaster Resilience (NIED) and universities (Figure 8). The JMA monitors the occurrence of earthquakes 24 hours a day. When an earthquake occurs, the JMA issues the Earthquake Early Warning, earthquake information and tsunami warnings/advisories based on the data.

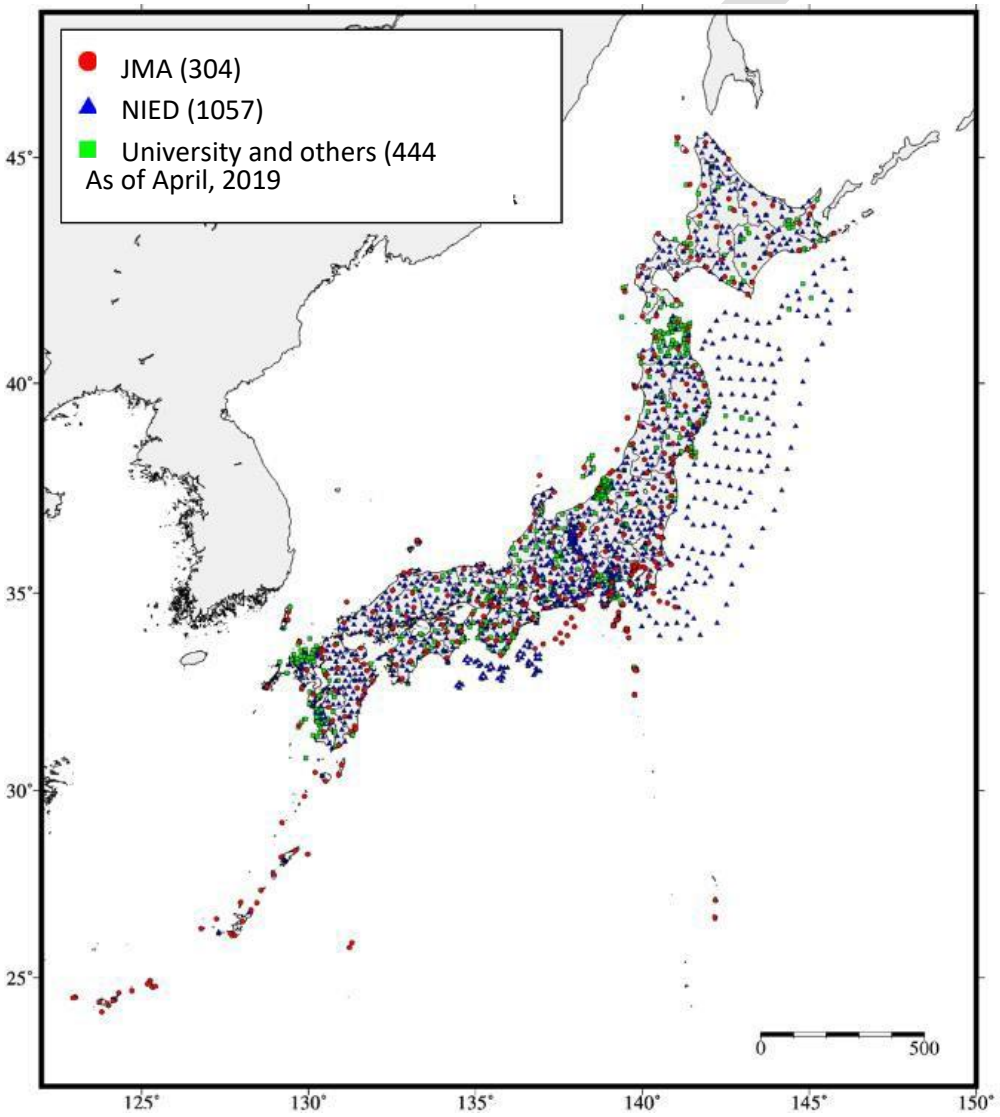

Figure 8: Map of seismic stations from which data are transmitted to JMA and used for EEW, tsunami warnings/advisories and earthquake information (as of April, 2019).

Real-time Sea Level Monitoring Network in Japan

Figure 9 shows the tsunami monitoring network around Japan, including offshore tsunami gauges. This network consists of tidal gauges along the coast, offshore GPS buoys (Kato et al. 2018; NOWPHAS (https://www.mlit.go.jp/kowan/nowphas/index_eng.html)), and ocean-bottom pressure gauges (DONET and S-net More than 400 stations are now operated by the JMA and other organizations. (see https://www.mowlas.bosai.go.jp/mowlas/?LANG=en).

Sea level data along the coast and offshore tsunami data are transmitted to the JMA on a real-time basis. The JMA uses the data in real-time tsunami monitoring and tsunami forecasting. If observed tsunami heights exceed forecasted tsunami heights, the JMA will update the first tsunami warning based on sea level observations as necessary (Ozaki, 2012).

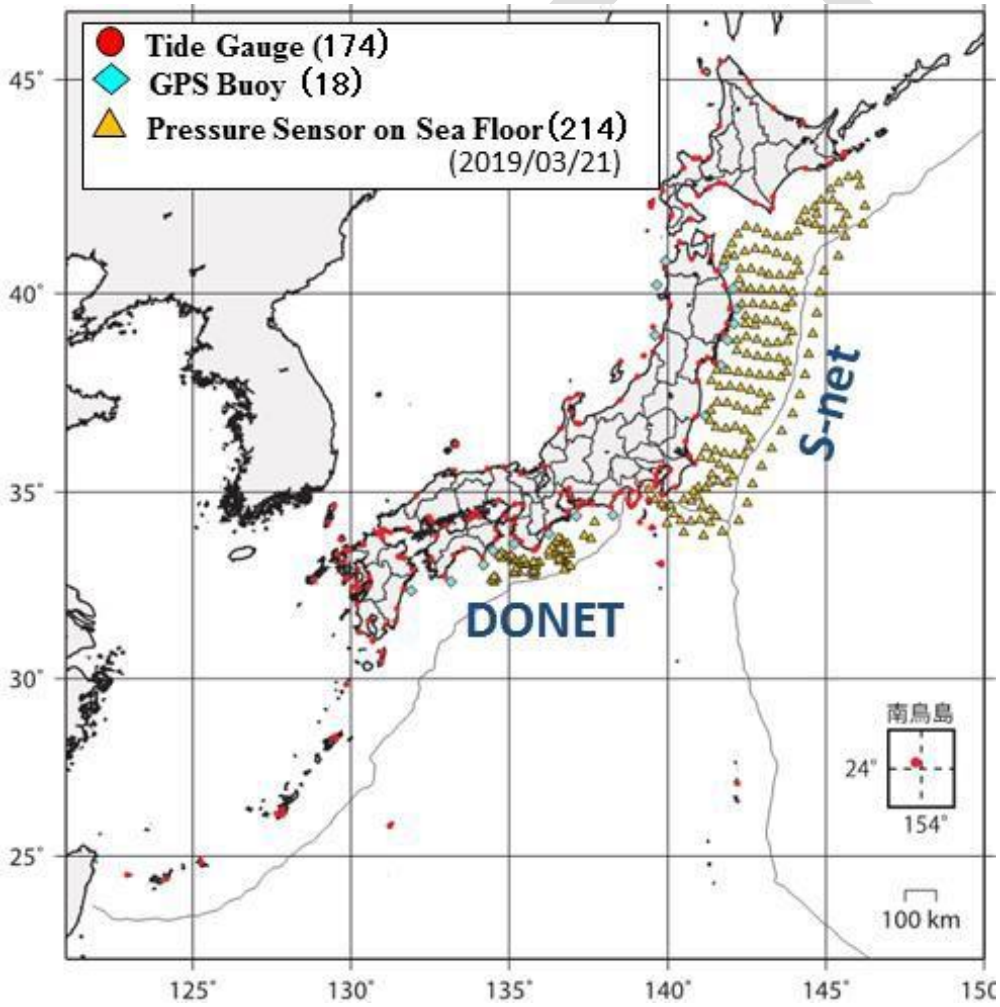

Figure 9: Distributions of tide gauges and offshore tsunami meters from which data are transmitted to the JMA on a real-time basis

Volcano observations

There are 111 active volcanoes in Japan (Figure 10). Some of them are island or marine volcanoes. Similar tsunamis to the Sunda Strait tsunami in Indonesia in 2018 may occur even in Japan. The JMA is monitoring volcanic activities using seismometers, GNSS observations and other methods (highly sensitive cameras, tiltmeters, infrasound sensors, infrared, volcanic gas). When JMA detects unusual phenomena, the JMA will issue volcano warnings and volcano information (Figure 11).

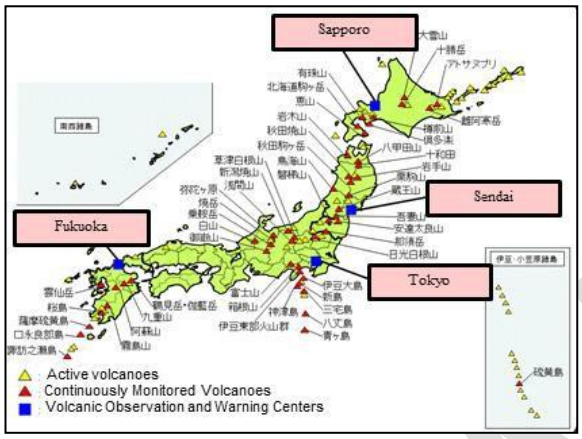

Figure 1:; Distributions of active volcanos in Japan

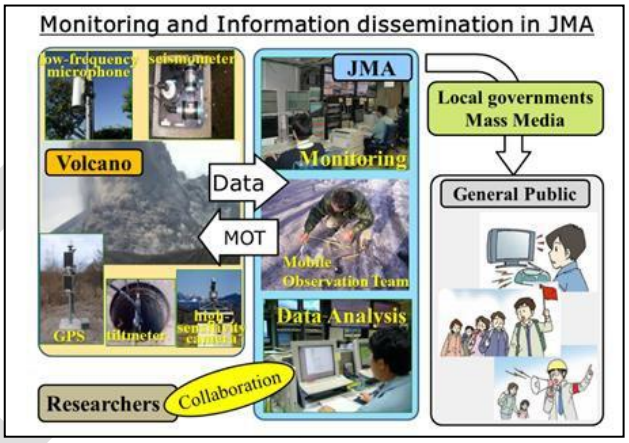

Figure 11: Monitoring system of volcanos and dissemination of information by JMA

The JMA operates meteorological satellites to monitor the atmosphere for weather forecasting and warning. The meteorological satellites have also been utilised for watching the diffusion of volcanic ash cloud for safety of navigation of aircraft as the Tokyo Volcanic Ash Advisory Center.

In 2019, Raikoke volcano in Kuril Islands erupted and generated a tsunami of concern. Figure 12 is the image of volcanic ash clouds accompanied with the eruption of Raikoke volcano.

Information on volcanic activity is shared between the volcanic section and the earthquake and tsunami section in JMA when there are concerns of tsunami generation accompanied with volcanic activities.

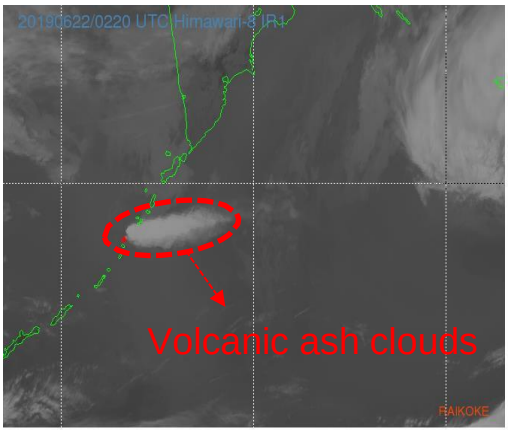

Figure 12: *Large eruption occured at Raikoke volcano in Kuril Islands in June 2019. The meteorological satellite (Himawari-8) of JMA captured volcanic ash clouds from the volcano.*

2.1.4 Norway – Rock slopes in fjords

It is well known that Norway fjords were frequently impacted by tsunamis induced by large rock and landslides failures. In particular, the fjords located close to Alesund were surveyed where two potential rock and landlide failures were identified (Aknes and Hegguraksla). The tsunami hazard due to these failures has been studied and major tsunami risks have been identified. Monitoring systems and contingency plans have been implemented for potential landslides for Åknes and Hegguraksla. These plans are established for actors with contingency responsibilities and tasks related to landslides from Åknes or Hegguraksla (last version in 2016).

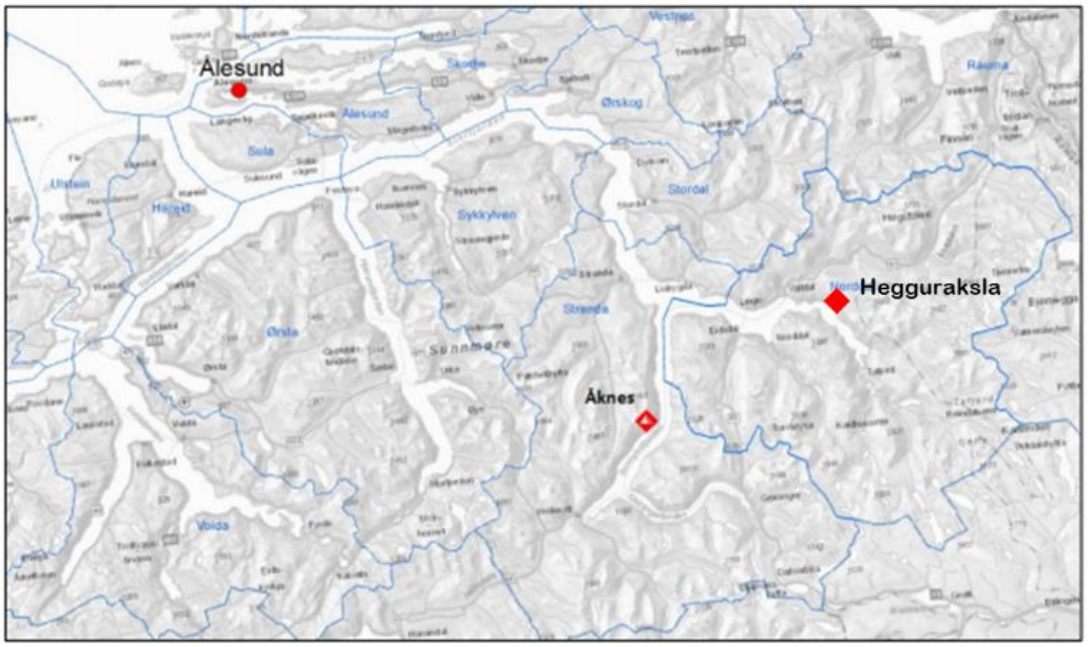

Figure 13: Alesund, Aknes and Hegguraksla location.

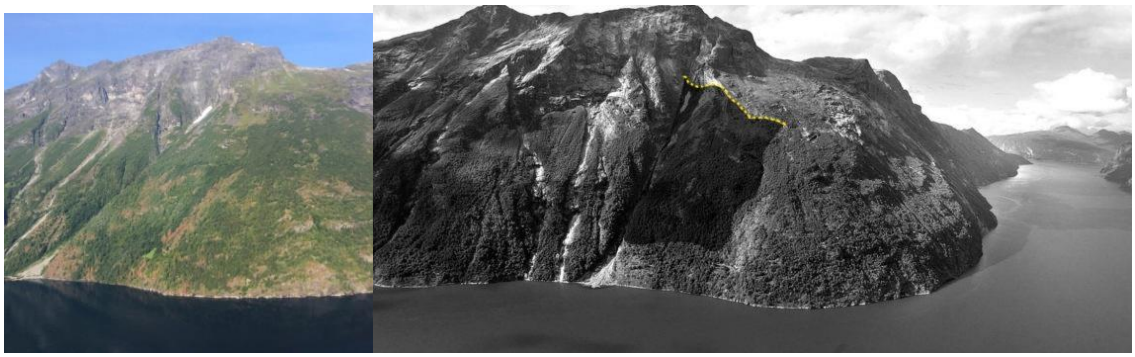

Figure 14: Pictures of the unstable mountain range at Aknes.

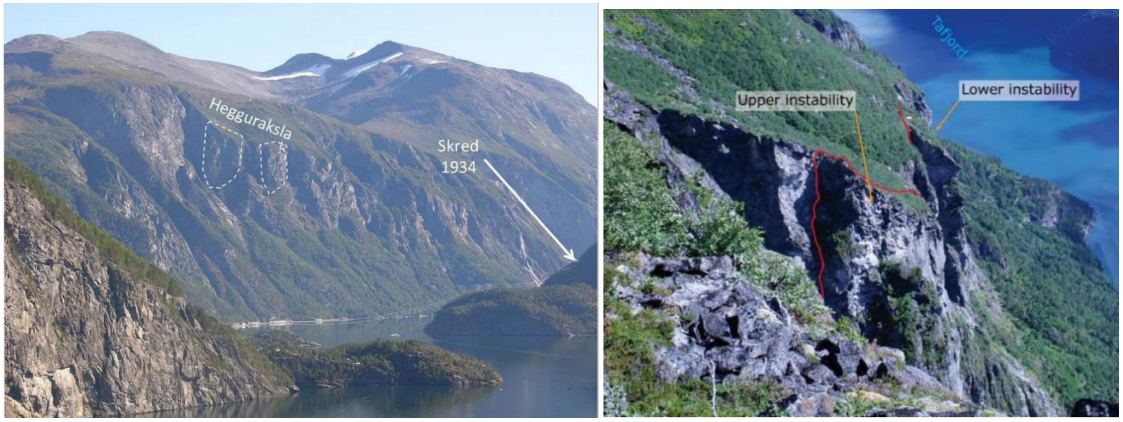

Figure 15: Picture of the two unstable mountain ranges at Hegguraksla.

The monitoring system implemented in the landslide zone includes various instrument networks (seismic, GPS, laser,…).

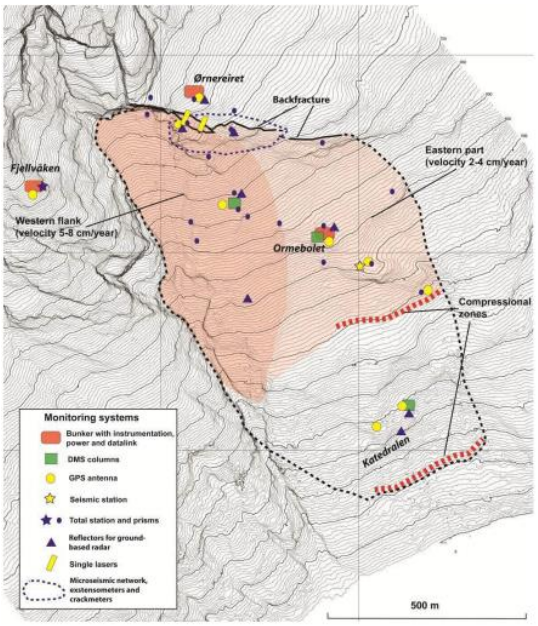

Figure 16: Map of monitoring network at Aknes

2.2 MODELING

The word ”atypical” brings together different sources of tsunamis (Table 4 and Figure 17) that require different strategies of modelling. The modelling of those tsunamis generated by earthquakes, is relatively well known and will not be presented in this report. Among all kinds of earthquakes related to volcanic and magmatic processes, only volcano-tectonic (high-frequency) earthquakes resulting from the accumulation of stress due to magma migration can involve ground deformation large enough to generate tsunami. They are characterized by seismic swarms at shallow depth (<10 km), with magnitudes typically lower than Ms = 6, except in the case of large-scale slumping of ocean islands (e.g., Ms = 7.2 Kalapana earthquake and tsunami at Kilauea volcano in 1975: Ma et al., 1999).

In the case of tsunamis caused by slope instability or volcanic activity, tsunami propagation can be simulated with depth-averaged models using the non-linear shallow-water equations or Boussinesq-type equations (Watts et al., 2003; Fritz et al., 2004; Yavari-Ramshe & Ataie-Ashtiani, 2016). Considering that atypical tsunamis are usually characterized by intermediate to deep-water waves (shorter wavelengths compared to tectonic tsunamis), it is highly recommended to use weakly dispersive depth-averaged models (Boussinesq type) or fully dispersive three-dimensional models (e.g., Reynolds-averaged, Navier-Stokes models). Near-field impulsive waves produced by subaerial geophysical flows typically transform into non-linear oscillatory waves, transitional waves, solitary- like waves, or dissipative bores (Fritz et al., 2004; Heller & Hager, 2011).

Tsunamis sources such as landslides or volcanic eruptions are often considered as “point sources” due to their limited dimensions (typically < 10 km²) compared to earthquake rupture areas (> 2000 km²). Consequently, it is important to consider the effect of spherical spreading in reducing wave amplitude with distance (Heller & Spinneken, 2015).

Source mechanism	% of events	Source volume km^3	Volume flux m^3/s
Underwater explosion	25	< 1	$< 10^9$
Pyroclastic flow	20	1-200	10^5-10^8
Earthquake	< 20		
Flank failure	15	1-500	10^5-10^6
Caldera subsidence	10	1-100	10^6-10^8
Air wave	5		
Lahar	< 5	< 1	$< 10^5$
Collapse of lava bench	< 1	< 0.01	$< 10^6$

* wave height at the shoreline

Table. 4 - The diversity of source mechanisms of tsunamis in volcanic setting (Paris, 2015; modified from Béget, 2000).

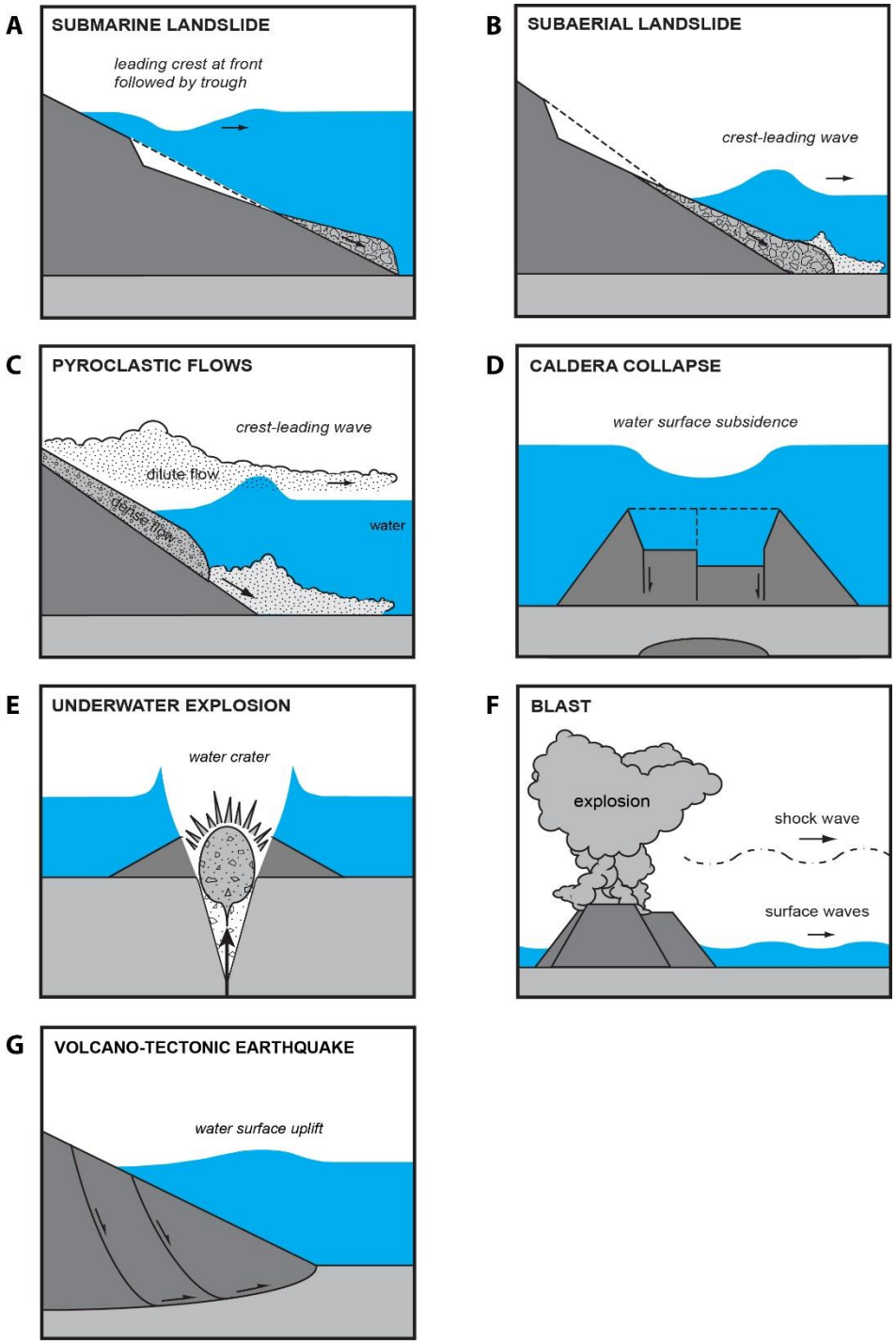

Figure 17: In the case of a volcanic eruption, tsunamis might be generated by landslides (A and B), pyroclastic flows (C), caldera collapse (D), underwater explosions (E), blast (F) or volcano-tectonic earthquakes (G) (modified from Paris et al., 2014).

The most critical part of the workflow is the treatment of the tsunami source. Atypical sources are characterized by different motions (from slow landslides or caldera collapses to almost instantaneous explosions), different geometries and configurations (submarine or subaerial flow, retrogressive, etc.),

rheologies (solid blocks, Newtonian and non-Newtonian flows), and combined sources (e.g., earthquake and landslide).

The choice of the model depends on the geometry and duration of the source, the quality of the available grid used for calculation (most atypical sources require a relatively small grid size compared to tectonic tsunamis), and the computing capacities. Sophisticated models such as dispersive, coupled flow/water models may have a very high computational cost. The modelling strategy is thus mostly guided by the objectives to be fulfilled. Understanding the physics or evaluating hazards will not require the same approach.

2.2.1 Landslides

Landslide tsunamis are particularly dangerous when generated in shallow waters and enclosed environments such as lakes or narrow bays, where they can produce very large localized runups (e.g., Lituya Bay tsunami, 1958). Their impact is more limited in the far-field. Key parameters in landslide tsunami generation differs depending on whether the slide is initiated offshore or onshore.

In the case of a submarine landslide (Figure 17a), the main parameters are the volume of the sliding mass, its initial acceleration, and its maximum velocity (Ward, 2001; Grilli & Watts, 2005; Harbitz et al., 2006). Tsunamis generated by submarine landslides display three successive waves: (1) A first crest ahead of the slide front, as a consequence of the energy transferred from the slide, (2) followed by a large trough propagating at the speed of the slide front, and (3) a final crest which represents the main cause of inundation (Yavari-Ramshe & Ataie-Ashtiani, 2016). Note that frequency dispersion is of little importance for tsunamis generated by large and subcritical submarine landslides (Harbitz et al., 2006).

Subaerial landslides are characterized by complex interactions flow/air/water at the impact, making them more challenging to simulate. The water above the flow is pushed upward, and the water in front is pushed forward (Figure 17b). The impulse (forced) wave first travels at the speed of the slide front, and then becomes a free wave (Lee & Huang, 2020). In the near-field, this leading wave is usually the largest one because it received most of the energy transferred from the slide at the impact. The height of the first wave increases with increasing slide Froude number, relative thickness, mass flux and volume (e.g., Fritz et al., 2004; Viroulet et al., 2013; Bougouin et al., 2020).

There are different types of methods for modeling landslide tsunamis. All these models are expert-dependent because the initial volume and geometry of the landslide (e.g., in one-go or retrogressive) are defined by the user:

- Empirical models are based on empirical equations that predict the characteristics of initial wave (height, speed, period, and length) and its evolution with propagation distance. These equations are based on the results of laboratory experiments (e.g., Heller & Hager, 2010; Heller & Hager, 2014; Mohamed & Fritz, 2012; Bougouin et al., 2020). This first-order approach is particularly efficient for a fast evaluation of the tsunami hazard.
- Static numerical models start from the definition of an initial water surface deformation, which is based on empirical equations (from observational or experimental data) (e.g., Watts, 1998; Satake & Kato, 2001; Grilli & Watts, 2005). Of course, these models neglect the kinematics and dynamics of the landslides.
- In kinematic numerical models, the motion of the landslide is assimilated to a time-dependent transient sea-floor deformation (e.g., Harbitz, 1992; Tinti et al., 2006; Iglesias et al., 2012; Paris

et al., 2020). The assumption that the underwater motion of the landslide can be used as a reliable initial condition is valid mostly for submarine landslides.

- Dynamic models correspond to more advanced coupled landslide-water models since the landslide is treated as a fluid flow with a given density, rheology, etc. The simplest approach is to define two layers in a depth-averaged model, the lower layer representing the landslide and the upper one the water (e.g., Imamura et al., 2001; Kelfoun et al., 2010; Giachetti et al., 2012). This approach is a good compromise between reliability and computing time. However, the complex hydrodynamics of landslide/water coupling requires fully dispersive models, especially in the case of subaerial landslides. Computational Fluid Dynamics (CFD) multi-fluid models using the Navier-Stokes equations are particularly recommended (e.g., Heinrich, 1992; Abadie et al., 2012; Ma et al., 2012; Grilli et al., 2019), but getting started requires special expertise and dedicated computing facilities. Smoothed Particle Hydrodynamics (SPH) are weakly compressible and meshfree Lagrangian models that can also be applied to the simulation of landslide tsunamis (e.g., Vacondio et al., 2013; Xenakis et al., 2017). In all these models, particle-fluid and particule-particule interactions are neglected. Discrete-element method (DEM) for simulating the landslide can be combined with a CFD method for the water (e.g., Zhao et al., 2016), but this approach is still at an initial stage of development and it has a huge computational cost.

2.2.2 Pyroclastic flows

Pyroclastic flows are hot mixtures of gas and particles generated by volcanic eruptions (Figure 17c), particularly in case of volcano dome collapse and plume collapse (Roche et al., 2013). There are historical and geological evidence of tsunami generated by pyroclastic flows (e.g., Krakatau 1883, Montserrat 1997 and 2003, Stromboli 2019). Several authors tried to simulate tsunamis generated by pyroclastic flows, using two-layers depth-averaged models designed for landslide tsunamis (e.g., Maeno & Imamura, 2011; Ulvrova et al., 2016).

However, the phenomenon of tsunami generation by a pyroclastic flow is complex for several reasons: (1) Pyroclastic flows belong to a category of highly-mobile flows due to an important gas pore pressure, (2) they are hot (typically 200-800°C) and might produce steam explosion when entering the water, (3) they are internally structured in a lower dense component and an upper dilute component, (4) and they are often heterometric (from block to ash-size clasts). Watts and Waythomas (2003) demonstrated that the most energetic and coherent water waves are produced by the dense, basal debris flow component of the pyroclastic flow. Preliminary reviews on tsunami generation by pyroclastic flows were presented by de Lange et al. (2001), and Watts & Waythomas (2003).

The important parameters controlling the interactions between pyroclastic flows and water bodies are the bulk density of the flow and its preservation offshore, the mass flux, the angle of incidence, and the distance from the shoreline (Cas & Wright 1991; Carey et al., 2000; Paris et al., 2014).

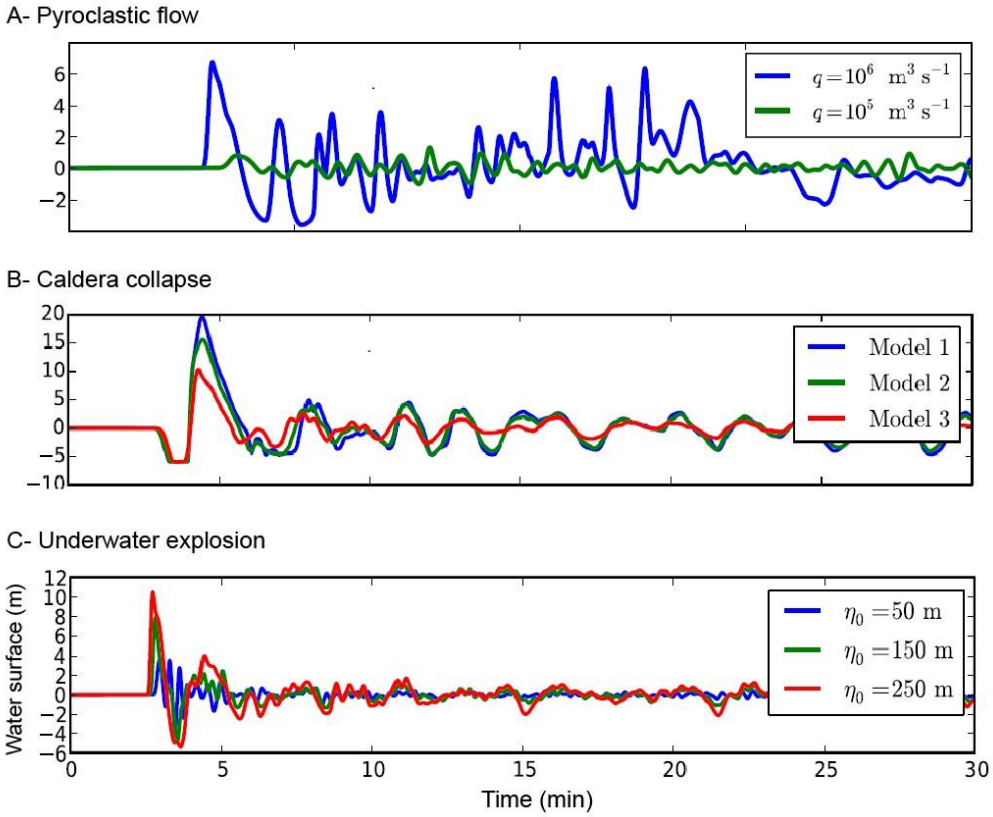

Figure 18 *– Water surface variations observed at the coast of Santorini for different types of tsunamis generated by an eruption of Kolumbo submarine volcano, Aegean Sea. (A) pyroclastic flow (plume collapse) with a volume V = 0.1 km³ and a discharge rate q = [10^5 : 10^6] m³/s entering the sea; (B) caldera collapse with different geometries (model 1 is a full-volume single-block collapse, model 2 is a half-volume single-block collapse, and model 3 corresponds to the deepening of a pre-existing caldera); (C) underwater explosions with different energies corresponding to initial water surface elevations η_0 = [50 : 250] m. Modified from Ulvrova et al. (2016).*

Experimental granular flows with a bulk density similar to water (e.g., pumice-rich flows) generate waves, whatever their temperature (Freundt, 2003). Experiments on fluidized granular flows by Bougouin et al. (2020) demonstrated that the wave features are mostly controlled by mass flux and the volume of the flow, unlike the water depth. This is confirmed by the simulations presented on Figure 18a, where a 10^6 m^3/s flow generates waves considerably larger than a 10^5 m³/s flow. The grain size may also affect the wave amplitude, as it controls the ability of water to penetrate the granular material (Bougouin et al., 2020). Interestingly, experimental fine-grained granular flows (e.g., ash-rich flows) behave as single-phase water flows in terms of wave generation. On-going experimental studies[1] on tsunami generation by pyroclastic flows will provide a robust background for numerical simulations based on CFD multi-fluid models.

[1] Contact Raphaël Paris at LMV (Laboratoire Magmas & Volcans, Clermont-Ferrand, France) for more information: raphael.paris@uca.fr

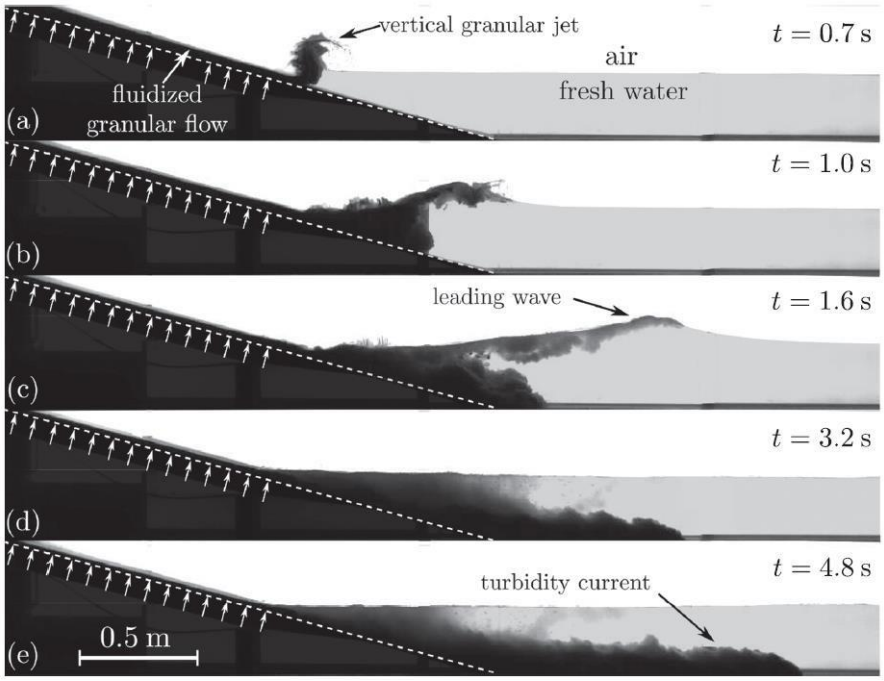

Figure 19 - *Snapshots of an experimental fluidized granular flow (i.e. pyroclastic flow) entering water at different times after gate opening at t = 0 (modified from Bougouin et al., 2020).*

2.2.3 Caldera collapse

Large explosive eruptions may result in the collapse of the central part of the edifice, thus forming a large depression, so-called caldera (Figure 17d). The diameter of a caldera typically ranges from hundreds of metres to several kilometres. The duration of a caldera collapse is poorly constrained (from minutes to hours) and the geometry varies from a single block to multi-stage subsidence of sub- blocks. In the case of a submarine volcano, the collapse first generates a subsidence of the water surface, which is immediately followed by a dome of water (e.g., Nomanbhoy & Satake, 1995; Maeno et al., 2006; Ulvrova et al., 2016).

Consequently, the wave train is characterized by a leading trough, followed by much larger positive crests (Figure 18B). The initial subsidence of the water surface depends on the geometry (diameter, depth, single- or multi-blocks) and duration of the collapse. Using a piston-like plunger model, Maeno and Imamura (2011) found that the water elevation above the caldera was the largest for a dimensionless collapse speed of 0.01 ($V_C^*=V_C/\sqrt{gh}$). With a similar approach, Ulvrova et al. (2016) tested different collapse geometries and durations, and they found that only fast (and unrealistic?) caldera collapses (<5 minutes) are efficient in terms of tsunami generation. Real-case caldera collapses usually last from ~30 minutes (e.g., Pinatubo 1991, Philippines) to 12 days (e.g., Fernandina 1968, Galapagos).

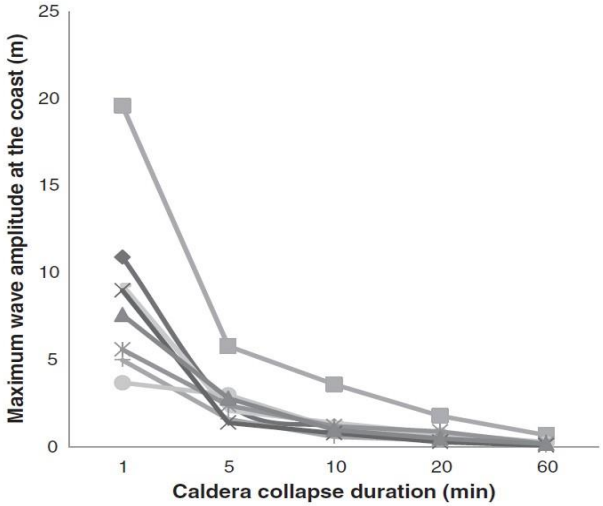

Figure 20: *Example of tsunami generated by a caldera collapse at Kolumbo volcano, Aegean Sea. The graph represents the maximum tsunami wave amplitudes recorded at the coasts of Santorini vs. duration of the caldera collapse (modified from Ulvrova et al., 2016).*

A complication in the field of volcanic tsunami comes from the fact that several tsunamigenic processes can be associated, thus complicating the interpretation of observational data (such as tide gauge records) and the definition of input parameters for numerical simulations. For instance, large caldera-forming eruptions may involve five tsunamigenic processes: pyroclastic flows, underwater explosions, earthquakes, the caldera collapse itself, and failures of the caldera walls (Paris, 2015). High discharge rate eruption of silicic magmas (e.g. rhyolite) during subaqueous caldera-forming eruptions might also generate pyroclastic ponds resulting in a dome of water rather than a subsidence (Cas & Wright, 1991).

2.2.4 Underwater explosions

The theory of waves generated by subaqueous explosions is well documented (e.g. Le Méhauté, 1971; Le Méhauté & Wang, 1996; Mirchina & Pelinovsky, 1988). This particular type of tsunami consists of two main positive waves followed by smaller undulations (Figure 17e) propagating radially from the source, as demonstrated by experiments (Le Méhauté & Wang, 1996; Kedrinskii, 2005) and numerical simulations (Torsvik et al., 2010; Ulvrova et al., 2014 & 2016; Paris & Ulvrova, 2019). The water is initially pushed upward, forming a crater with a cylindrical bore that expands radially to form the leading wave, followed by a wave trough. Initial surface displacement (i.e., maximum height of the bore) can be estimated directly as a function of explosion energy at a given water depth (Le Méhauté, 1971), or indirectly using the size of the submerged volcanic crater formed by the successive explosions (Sato & Taniguchi, 1997; Goto et al., 2001). The water crater collapses as in a dam break model, generating a steep dome of water that turns to a second cylindrical bore (Le Méhauté & Wang, 1996). Underwater explosions typically generate short- period waves, and most of the time the impact in the far-field is limited (Paris, 2015). For simulating the tsunami propagation, it is thus recommended to use dispersive models.

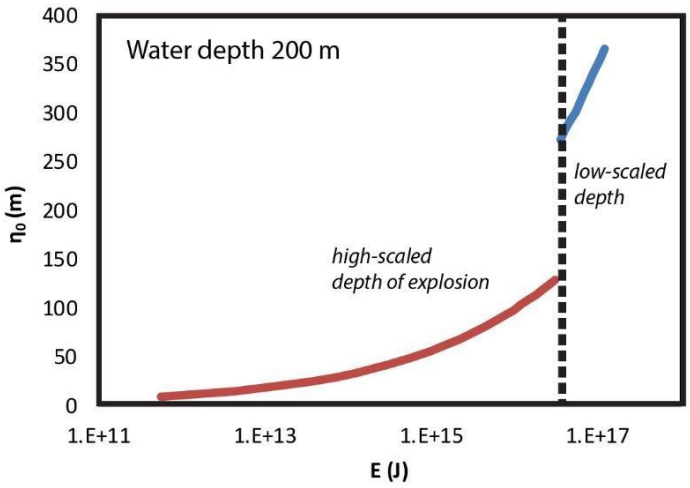

Figure 21 – Relationship between the explosion energy and the initial water surface displacement (calculated from the empirical equation of Le Méhauté, 1971). Two cases of explosions should be distinguished: deep explosions with a high-scaled depth of explosion (compared to a water depth of 200 m in this case), and shallow explosions with a low-scaled depth (Le Méhauté & Wang, 1996).

For simulating the tsunami source, we recommend a semi-analytical approach that neglect complex interactions between dispersed fragments of lava, gas bubbles and water (which would require extremely complex multi-phase models). The underwater explosion is approximated by imposing a specific initial water surface displacement (η_0) that depends on the explosion depth and energy released during the explosion (e.g., Torsvik et al., 2010; Ulvrova et al., 2014). Initial surface displacement mostly depends on the depth and energy released during the explosion. There exist purely empirical relations that estimate η_0 as a function of explosion energy (e.g., Sato & Taniguchi, 1997; Goto et al., 2001). In order to have a homogenous circular source at the apron of the explosion, it is recommended to use fine grid resolution or to refine the available grid. A poor resolution of the source (few pixels) might generate artificial directivity of propagation (Paris & Ulvrova, 2019).

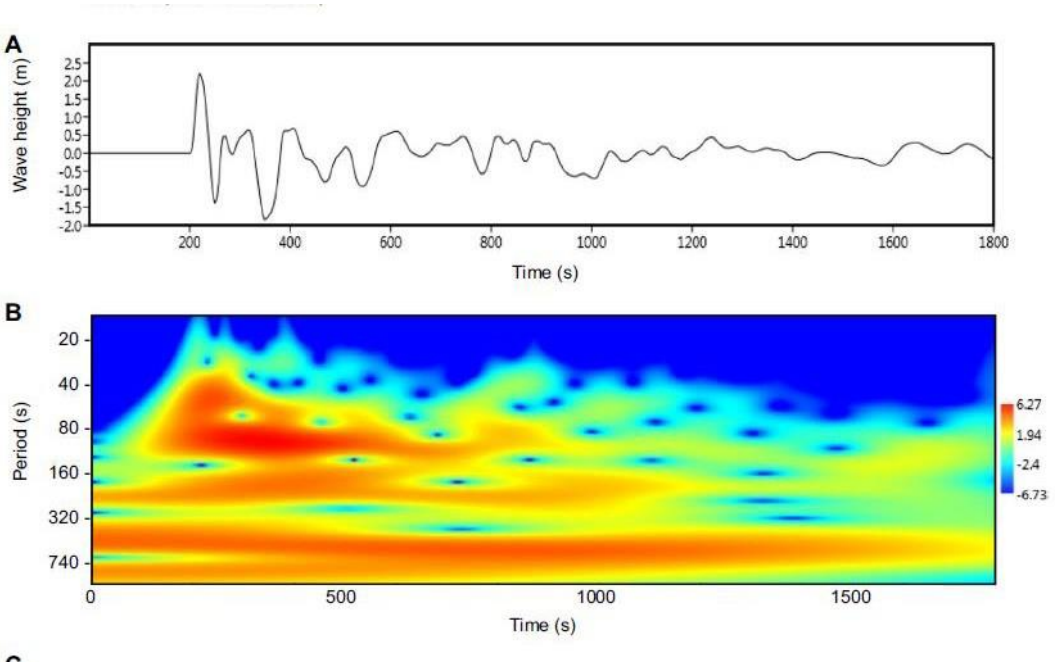

Figure 22 *- Spectral analysis of a tsunami generated by an underwater volcanic explosion in Taal Lake (Philippines). A: wave height vs. time profile; B: wavelet power spectrum (continuous wavelet transform). Modified from Paris & Ulvrova (2016).*

Tsunami source	**Geometrical parameters**	**Dynamic parameters**
Submarine landslide	slide volume, water depth	initial acceleration
Subaerial landslide	slide volume, front thickness	slide Froude number, mass flux
Pyroclastic flow	flow volume, front thickness	flow Froude number, mass flux
Caldera collapse	collapse geometry (e.g. aspect ratio), water depth	collapse duration (usually >30 min)
Underwater explosion	scaled explosion depth (deep or shallow compared to water depth)	explosion energy (can be estimated from crater size)

Table 5 – Relevant parameters to be considered in numerical simulations of atypical tsunamis. Note that parameters for subaerial landslides and pyroclastic flows are similar, but the pyroclastic flow is characterized by a higher mobility.

2.3 HAZARD ASSESSMENT

2.3.1 Italy – Stromboli

Since the early 20th century, six tsunamis generated by landslides within the Sciara del Fuoco (SdF) of Stromboli have been reported (Maramai et al., 2014). The last significant tsunami event occurred on 30 December 2002 as a consequence of the collapse of both aerial and submerged large portion of the SdF (Tinti et al., 2006 a,b; Chiocci et al., 2008; Fornaciai et al., 2019). The waves, with runup reaching about 10 m along parts of the coast of Stromboli, caused significant damage to the buildings located near the beaches of Stromboli, but also reached the nearby Panarea island and the Southern Tyrrhenian Sea coasts (Maramai et al., 2005; Tinti et al., 2005, 2006a).

In the last decade, several research activities have been focused on identifying the most effective modeling approach (in terms of accuracy and computational efficiency) for the tsunami generation and propagation in an active volcanic context, and, in particular, towards the island of Stromboli (Selva et al. 2021; Esposti-Ongaro et al., 2021). To this aim, Stromboli tsunamis have been studied using different benchmarked models, with different levels of approximation and accuracy: the NHWAVE three-dimensional non-hydrostatic model in sigma-coordinates (Ma et al., 2012) and the HySEA family of geophysical codes (Macías et al., 2015) based on either single layer, two-layer stratified systems or multilayer non-hydrostatic formulations of the wave model (Fernández-Nieto et al., 2008). Concerning the source, both rigid and deformable submarine landslide models, with volumes ranging from 6 to 20 million cubic meters, have been used to trigger the water waves.

The comparisons among models have targeted differences in terms of maximum run-up, inundation in the area of the village of Stromboli, and of waveform at four proximal sites (two of them corresponding to the locations of the monitoring beacons, offshore the SdF). Hydrostatic and non- hydrostatic models show that the simulated inundation maps at the Stromboli village are relatively similar. On the other hand, preliminary results indicate strong differences between the proximal waveforms, as quantified by the different considered models. Such differences were expected, due to frequency dispersion and other model differences, as subaerial landslides almost invariably generate dispersive waves (e.g., Løvholt et al., 2015). The results show that the use of non-hydrostatic models allows better describing proximal waveforms.

However, in terms of hazard quantification, the source description remains the most sensitive (and uncertain) aspect of the modeling, plus non-hydrostatic models are computationally more expensive than hydrostatic ones. This complicates the extensive exploration of source variability. The use of High-Performance Computing (HPC) techniques, and in particular of Graphic Processing Unit (GPU) accelerators for the numerical solution (Macias and de la Asuncion, 2019), have now allowed much faster simulations, opening a new avenue for probabilistic tsunami hazard assessment and, possibly, tsunami early warning (Lovholt et al., 2019b).

Even if fully probabilistic tsunami hazard quantifications are not yet available for Stromboli, tsunami modelling has strongly contributed to the definition of the hazard and to the calibration of the tsunami warning system. A dataset of synthetic scenarios with varying landslide volumes, initial height of the center of mass, and landslide-water density ratio has been produced, allowing a deeper investigation of the potential impact of landslide-induced tsunamis along the coasts of Stromboli. On the otherhand, the waveforms produced with a non-hydrostatic model have been used to provide a preliminary calibration of the tsunami alert system of Stromboli and its automatic detection algorithm.

2.3.2 Indonesia – Anak Krakatau

Anak Krakatau is a volcanic island located in the Sunda Strait (Indonesia), which emerged in 1927 on the rim of the submarine caldera that was formed during the 1883 eruption of Krakatau. The position of the volcano on a steep slope motivated Giachetti et al. (2012) to simulate a hypothetical collapse of the

southwestern flank of the volcano. The simulated tsunami would reach the communities located on the western coast of Java 35 to 45 min after the onset of collapse, with a maximum amplitude of 1.5 m (Merak, Panimbang) to 3.4 m (Labuhan), then Bandar Lampung (Sumatra) after >1 hr, with a maximum amplitude of 0.3 m. Giachetti et al. (2012) warned that such an event would likely cause significant damage around the Sunda Strait due to high population, and a concentration of road and industrial infrastructure at the coast. Paris et al. (2014) reminded that "Krakatau still represents a tsunami hazard for the coasts of the Sunda Strait", and they concluded that "a rapid detection of volcano instability by the observatory together with an alert system on the coast could prevent a hypothetical tsunami from being deadly." As a consequence, tsunami evacuation routes along the Java coast of Sunda Strait have been in place since 2008.

However, on 22 December 2018 the southwestern flank of Anak Krakatau collapsed into the sea and generated a tsunami in the Sunda Strait, killing 431 people and damaging thousands of houses and boats. Although such a scenario had been predicted by Giachetti et al. (2012), the disaster could not be prevented and became one of the deadliest volcanic eruptions over the last several decades. Although the volcano was particularly active before its collapse, an alert was not issued because: (1) Volcanic eruptions were not able to be included as potential tsunami sources in the tsunami early warning system, and (2) there was no formal communication proceduers on tsunami hazard associated with volcanic activity between the two key institutes (Badan Meteorologi, Klimatologi, dan Geofisica (BMKG) for tsunami warning, and Pusat Vulkanologi dan Mitigasi Bencana Geologi (PVMBG) for volcano monitoring). The tsunami also arrived during the dark of the evening, making it difficult for people to observe the incoming waves and self-evacuate.

2.3.3 Other hazard assessments – Greenland

Since 2000, two tsunamis have occurred along the western coasts of Greenland, due to subaerial coastal landslides. The 21 November 2000 tsunami related landslide (Dahl-Jensen et al. 2004), consisted of a large volume of 90 million m^3 of rock, sliding at Paatut, between altitudes of 1400m and 1000m, of which 30 million m^3 sunk into the ocean. The resulting tsunami reached a height of 50m at the source, and inundated 250m for a runup of 28m at the village of Qullissat. The second one occurred on 17 June 2017, was similar and located 150km north of the 2000 event. The tsunami flooded several villages up to a distance of 160km away, killing 4 people, injuring 9 and destroying 11 houses in the village of Nuugaatsiaq. This tsunami was also triggered by a subaerial landslide which occurred in a fjord 32km ENE of Nuugaatsiaq on the Northern slope of the Karrat Fjord. The 2017 event consisted of a large volume of 58 million m^3 of rock, sliding between altitudes of 1200m and 800m, of which 45 million m^3 reached the water (Paris et al. 2019).

These kinds of events should be considered as a recurring hazard in that region, in particular in the western parts of Greenland.

A potential landslide next to the 2017 event was identified as threatening Karrat Fjord. A sensitivity study on different scenarios was undertaken on its volume, with 2-38 million m^3 reaching the sea (Paris et al. 2019). The results show a 7 million m^3 slide corresponding to a potentially hazardous tsunami at Nuugaatsiaq. Later, this village was been definitively evacuated.

The Greenland events make it clear that such kinds of sensitivity studies could be performed to assess the local tsunami hazard in fjords and bays to assess where some mass instability should be considered as a threat for villages and marinas located in the region.

Such a study should take into account the potential volume of the slide, its location and altitude, and the rheology of the sediment/roc.

2.4 WARNING

2.4.1 Italy – Stromboli

The tsunami acoustic warning system of Stromboli has been in operation since 2003 and its first activation occurred on 27 February 2007 (Bertolaso et al., 2009). The system has both manual and automatic activations. Automatic activation has been made operational only recently, and it is based on real-time tsunami detection. A tsunami detection algorithm has been implemented using the ratio between Short-Term and Long-Term Averages (STA/LTA; Lacanna and Ripepe, 2020; Selva et al. 2021a). Theoretically, the algorithm is able to automatically detect tsunami waves in any sea condition, since tsunami signals produce STA/LTA values well above the identified threshold. The first successful test was performed on 3 April 2019. A first real-time testing happened during July and August of 2019, when two small tsunamis were generated by pyroclastic flows following paroxysmal explosions (Figure XXX) and the automatic system was still in its testing phase. The system is now operational, after final testing occurred on 9 September 2019.

The acoustic warning system is composed of 8 sirens (in Stromboli, as well as in the nearby island of Panarea) and one beeper (at the Coast Guard premises in Sicily), inter-connected by a dedicated radio network (VHF band), and three main base stations (radio links) located in Antennamare (Province of Messina, in Sicily), Stromboli and Panarea, which allow the simultaneous activation of the above-mentioned sirens (Dipartimento della Protezione Civile and Regione Sicilia, 2015).

A management software system that runs on a workstation located inside the COA gives the opportunity to select three possible combinations for the activation of the acoustic system:

- Single: activation of one siren (out of the nine available);
- Group: activation of pre-selected group of sirens (i.e., only Stromboli group or Panarea group);
- Global: activation of all the sirens.

The first national civil protection emergency plan for the volcanic events generated at Stromboli was issued in 2003, just after the 30 December 2002 tsunami. The plan was updated in 2015, taking into account new scenarios and the introduction of the national volcanic alert level system. The 2015 plan (Dipartimento della Protezione Civile and Regione Sicilia, 2015) considers as tsunami inundation zones those caused by the 30 December 2002, as defined by site observations and measurements (Maramai et al., 2005; Tinti et al., 2006a; Bertolaso et al. 2019). This event is, to date, the best documented in terms of impact on the island, and the most significant that has occurred in recent times. This area is densely inhabited, and in terms of emergency management it represents an exposed area that will be evacuated in case of: i) evidence of intrusion and deformations in the SdF, which can lead to a possible collapse and subsequent tsunami; and ii) automatic activation of the acoustic warning system (sirens) after the detection of a tsunami. Noteworthy, it is in place also as an automatic early warning system for paroxysmal explosions (Ripepe et al., 2021). This system triggers sirens locally at Stromboli and Ginostra (Dipartimento della Protezione Civile and Regione Sicilia, 2015). The tsunami early warning system is instead automatically triggered only when a tsunami is detected by the MEDAs and activates the entire network of sirens.

The sirens have two different acoustic signals assigned to each phenomenon: i) bi-tonal for paroxysmal explosions and ii) mono-tonal for tsunamis.

In case of tsunami, evacuation routes have been identified to reach the gathering points and guide people to the safe areas (Figure 23). Each evacuation route has its own emergency signals explaining the correct path to follow. More details can be found in Dipartimento della Protezione Civile and Regione Sicilia (2015).

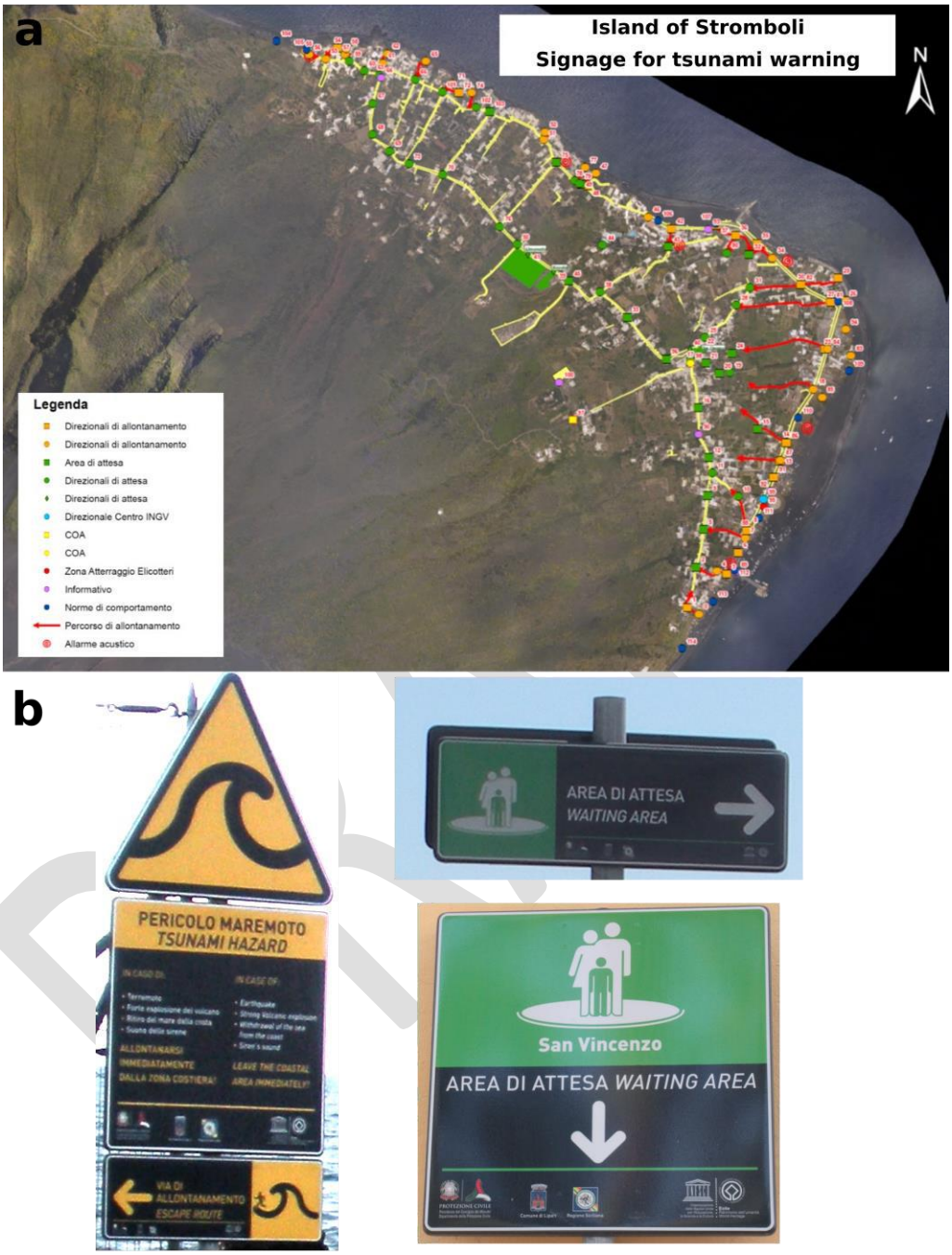

***Figure 23**: Signage connected to the Tsunami Warning System: (a) map of the signage in Stromboli village; (b) examples of signage for instructing to evacuation in case of major explosions and tsunami detection (photos curtesy of Dipartimento della protezione civile)*

2.4.2 Indonesia – Anak Krakatau

Learning from the Sunda Strait tsunami on 22 December 2018, the Indonesian government tried to be more active in dealing with such disasters.

Since 2019, BMKG and PVMG are coordinating and collaborating together under the Indonesian Presidential's Decrees Number 93. The monitoring of volcanic activities and landslide is being conducted by PVMG and BMKG, who are developing and implementing methods for tsunami modelling, monitoring, and warning. Monitoring will consist of several sea level sensors around the Sunda Strait, ocean bottom pressure gauges (OBPG), tide gauges, and radar. A new InaTNT (Indonesia Tsunami Non-Tectonics) system will be tested, with the aim of providing tsunami warnings to the community based on preliminary records of ocean waves around the Anak Krakatau volcano. InaTNT is a sea-level anomaly detection system that indicates tsunamis with a detection method based on earthquake characterization. InaTNT detects sea level onset at a certain period with the STA / LTA method. Each trigger generated will activate the alert and notification system on the InaTNT GUI system.

Sirens are implemented with the alert being issued if wave measurement exceeds 0.5 m. BMKG sends earthquake information and tsunami to local DMO (Disaster Management Office) with 3 levels of warning: (i) major warning (estimated tsunami is more than 3m); (ii) warning (estimation tsunami height is 0.5-3m); (iii) advisory (estimation of tsunami height is less than 0.5m). When the alert is considered as major, BMKG recommends immediate evacuation, but local DMO makes the final decision depending on local conditions and specificities.

2.4.3 Japan – JMA

The Japan Meteorological Agency (hereinafter, JMA) is the sole organization for issuance of tsunami warnings in Japan. JMA's tsunami warning system is applied to typical tsunamis generated by an earthquake. In addition, JMA is responsible for issuance of tsunami warning for atypical tsunamis generated by a non-seismic source. In this report, JMA's tsunami warning system to atypical tsunamis will be introduced.

Tsunami Forecast System for Tsunami Warning

Tsunami warnings have to be announced quickly, before a tsunami reaches to the coast. The target time for issuance of a tsunami warning is about 3 minutes after occurrence of the earthquake in case of a near-field tsunami. To achieve this purpose, JMA have implemented the "Database method" (Kamigaichi; 2015). Because even if computer simulations start after the occurrence of each earthquake, there is not enough time left for issuance of a warning. About 100,000 tsunami scenarios are assumed around the Japan archipelagos in the database. When an earthquake occurs, the location and magnitude are quickly estimated, and the system just searches the possible scenarios from the database and tsunami warnings or advisories at coasts are issued accordingly (Figure 24). Using this method, JMA can issue a tsunami warning within about 3 minutes after the occurrence of an earthquake.

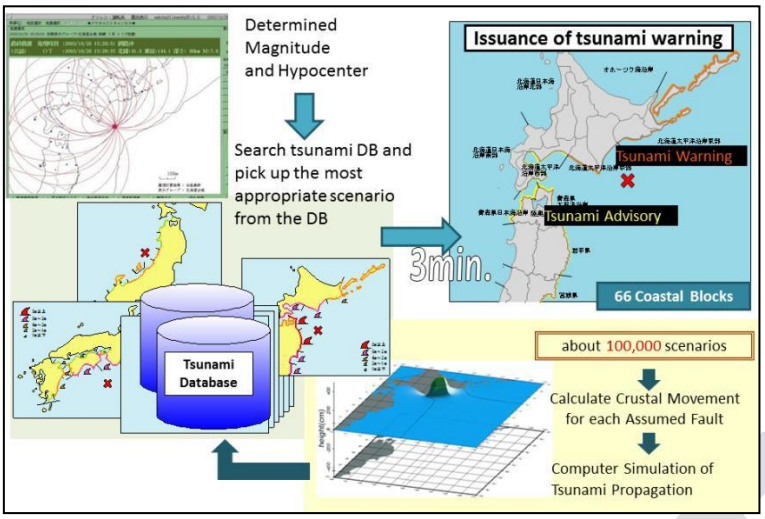

Figure 24 : Tsunami forecast system of the JMA for the first tsunami warning

Tsunamis generated by non-thrust type earthquakes

The fault type in the database is a pure reverse fault with a dip angle of 45 degree and slip angle of 90 degree. Other types of earthquakes, such as a normal fault, certainly occur around Japan, as well as a strike slip fault. A pure reverse fault can effectively generate a higher tsunami than other types of fault. In view of disaster management, JMA applies the database to other types of earthquake for a tsunami warning, including a strike slip fault. JMA must issue a tsunami warning within about three minutes. But the characteristics of the earthquake cannot be identified in such very short time. Assuming the more conservative case, JMA issues a tsunami warning.

Tsunamis generated by volcanic sources

The JMA's "Database method" cannot be applied to tsunamis generated by non-seismic tsunamis, such as volcanic avalanches (landslides). JMA does not have generalized procedures for tsunami warning for volcanic tsunamis. When a volcano gets more active and generation of tsunamis becomes a concern, the JMA implements tsunami warning procedures according to expected tsunamis. Concrete procedures have to be made case-by-case according to activities of the targeted volcano. Because in case of a tsunami caused by an earthquake, JMA can quickly obtain source parameters using CMT analysis and other methods and JMA can simulate tsunami propagation using an advanced computer. However, in a tsunami caused by volcanic avalanches, even if JMA can detect volcanic avalanches, it is difficult to quantitatively estimate the size of tsunami source and tsunami heights at the coast. Volume, speed and direction of avalanches can not be confirmed in a short time after the occurrence. So, it is difficult to issue quantitative tsunami warnings for such an event.

JMA is monitoring volcanic activities using seismometers, GNSS observation and other methods. If JMA detetcs unusual behaviour, JMA will issue volcano warnings and volcano information. Information on volcanic activities is shared between the volcanic section and the earthquake and tsunami section of JMA

Every time volcanos become active, the JMA prepares for tsunami warnings. In order to

determine the criteria and procedures for issuance of a tsunami warning, JMA takes their own model into consideration with various cases and the tsunami is simulated. Targets of tsunami warning are coastlines near an island/marine volcano with certain activity level. JMA estimates tsunami height using tsunami simulations to the targeted coasts in advance under various conditions, as well as arrival times of the tsunami using tsunami propagation charts.

The issuance condition of a tsunami warning is that an earthquake occurs near the volcano, a volcanic avalanche or collapse of a volcano are detected by camera and/or GNSS buoys, and ocean bottom pressure sensors and tide gauges record tsunami wave activity. If the conditions which are determined in advance are satisfied, JMA issues pre-determined tsunami warnings for the targeted coasts as early as possible. If tsunamis are observed at GNSS buoys, ocean bottom pressure sensors and tide gauges, they may exceed the predicted tsunami height. The JMA will then update tsunami warning based on observed heights, if necessary. However, volcanic avalanches are not always detectable with cameras or other monitoring instruments.

Summary

It is difficult to detect the occurrence of atypical tsunamis. Offshore tsunameters are useful tools for early detection of atypical tsunamis.

Strong and close collaboration with the volcano observation authority is essential for early warning for tsunamis caused by the explosion and collapse of a volcano. Public should be made aware of the possibility of tsunami generation caused by explosion and collapse of a volcano and landslide, as well as a tsunami generated by an earthquake.

Detection of a submarine landslide needs a dense network in all seismic zones. Japan and JMA have implemented and maintained a dense seismic network. The seismic network so far has been not used for warning operations to tsunamis generated by a landslide, because seismic waves generated by a landslide are too small in comparison with the seismic waves by the former shock. Seismic records of landslides are therefore masked by seismic records of the former shock. Methods for identification of landslides and characterizations such as amount of volume and direction of the landslide should be developed, along with methods for estimating of the size of tsunamis for practical use in tsunami warnings.

2.4.4 Norway – Acknes and Hegguraksla

Contingency plans have been established, for Aknes and for Hegguraksla rock slides.
Both plans are based on the results of hazard modeling studies, in particular propagation maps and maximum height of tsunami waves for extreme case scenarios (Figure 25 and 26).

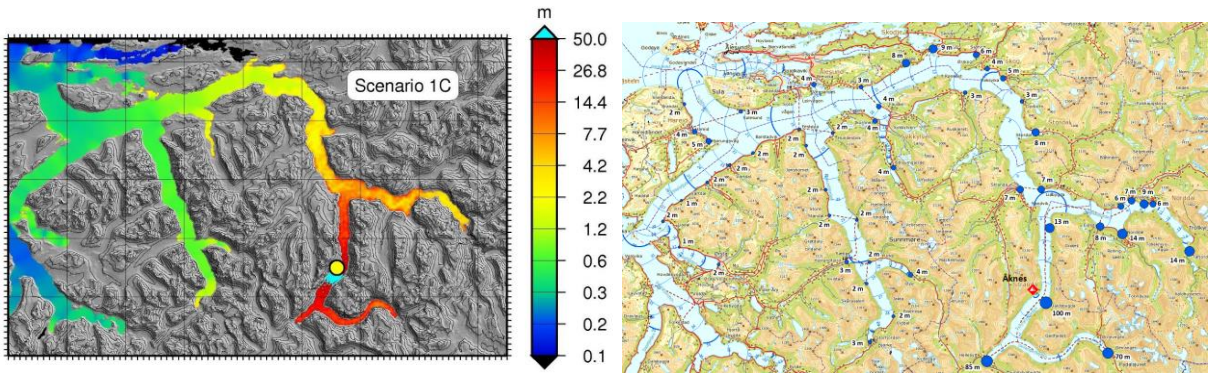

Figure 25 : Maximum surface elevation and travel time in the fjord by a landslide from Aknes with a volume of 54 mill m3

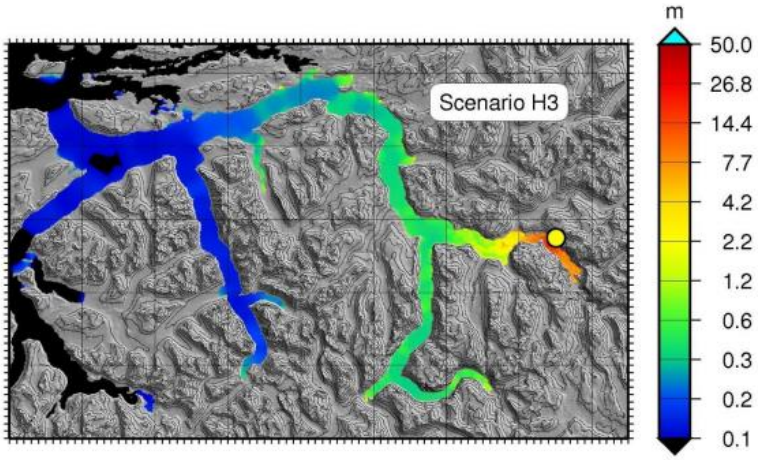

Figure 26 : Maximum surface elevation in the fjord by a landslide from Hegguraksla with a volume of 3.5 million m3

In the contingency plan, four different danger levels have been established: Green, Yellow, Orange and Red (Table 6).

GREEN HAZARD LEVEL normal situation. No avalanche is expected in the near future (weeks/months). The on-call geologist evaluates the condition of the monitored rocks once a day. If the speed of the mountain exceeds the given threshold values, the geo-guard is automatically notified.
YELLOW DANGER LEVEL means that there is an increased risk of avalanches, but an avalanche is not expected until a few weeks, perhaps somewhat longer. The on-call geologist checks the condition of the mountain range at least every two hours. The police, municipalities, nve etc. keeps in close contact. Yellow hazard levels normally do not result in any mandatory relocation or evacuation measures, but preparations will be initiated for measures taken at higher hazards.
ORANGE DANGER LEVEL means that the probability of an avalanche has increased further, and an avalanche is expected to occur within a week, perhaps somewhat longer. The state of the mountain party is evaluated continuously, 24/7. During this phase, the municipality will relocate vulnerable businesses such as kindergartens, schools and health institutions. Fish cages within the danger zone are moved to reserve sites outside the danger zone. Fjords will be closed to shipping.
RED DANGER LEVEL means that an imminent avalanche is very likely. The mountain range is evaluated continuously, 24/7.This hazard level should be notified no later than 72 hours before an avalanche, and evacuations must be completed no later than 12 hours after the red hazard level has been notified. When red hazard levels are notified, the police will immediately initiate evacuations of defined evacuation zones. Roads, railways and other traffic within the danger zones will be closed.

Geologisk situasjon	Farenivå	Beredskapsnivå og -tiltak
Stabil bevegelse med sesongvariasjoner	Lav fare	**Grønn beredskap:** • Overvåking • Planlegging • Øving
Økt bevegelse, utover sesongvariasjon	Moderat fare	**Gul beredskap:** • Intensivert overvåking • Gjennomgang av planverk • Aktivering av samordningsfora • Forberede komplekse tiltak • Informasjonstiltak
Akselererende bevegelse	Høy fare	**Oransje beredskap:** • Intensivert beredskap • Flytting av sårbare objekt • Reduksjon av aktivitet og ferdsel
Skred nært forestående	Ekstrem fare	**Rød beredskap:** • Evakuering • Redning
Skred har gått, kan gå igjen		**Rød beredskap:** • Opprettholdelse av evakuering • Reetablering av overvåking

Table 6: Four levels of danger

2.4.5 Emergency Management perspective

Public education with regards to evacuation for atypical tsunami sources is particularly challenging and hence not practical, due to:

- The likely lack of commonly experienced natural warning signs associated with atypical sources, i.e., felt seismic shaking. Where visible or noise warning signs may be present, it is likely to be variable/inconsistent depending on the source; and will also likely be observed too late to support effective evasive action.

- The infrequent and variable nature of such events.

Effective evasive action and response will therefore depend almost solely on official warnings. Consideration of atypical sources in tsunami warning planning is therefore important, particularly with a view on the following:

- A common understanding between monitoring, warning, and emergency management agencies about the presence and potential of atypical tsunami sources, and the responsibilities between them for the monitoring, assessment, decision making, warning, and subsequent response actions. Clear communication between these stakeholders is essential in the observation, analysis, and decision-making process, especially noting that more stakeholders will likely be involved than for typical tsunami sources (i.e., the responsibility for seismic, volcanic, and atmospheric monitoring may be located with different stakeholders).

- Because of the likely absence or less effective instrumental monitoring capability for atypical sources, combined with a likely less developed understanding of these sources in terms of tsunami potential, there will likely be higher degrees of uncertainty with regards to the likelihood of tsunami generation and the size (wave height) if a tsunami has been generated during atypical events. The effective warning time and the areas to be placed under warning will also be impacted by this uncertainty (as well as by the location of the source). Planning will therefore have to take a more conservative approach in comparison to typical tsunami sources (where monitoring and understanding is generally better developed).

3. METEOTSUNAMI

Meteotsunami or meteorological tsunamis are atmospherically-generated long ocean waves in a tsunami frequency band, found to occur in all the world oceans and basins (Monserrat et al., 2006; Rabinovich, 2020). Travelling atmospheric disturbances observed in air pressure and wind may,

through a multi-resonant amplification, reach sea level oscillations with wave heights of several metres that may be particularly dangerous in micro-tidal regions and narrow constrictions.

Several monitoring and warning systems are currently under development or being operational in the world, like the Balearic RIssaga Forecasting System (BRIFS; Renault et al. 2011) and the Adriatic Sea and Coast (AdriSC) system (Denamiel et al. 2019a, b) (Figure 27). They may consist of several modules: (i) high-frequency (a minute time resolution) sea level and air pressure (wind) observations in the area affected by meteotsunamis, (ii) deterministic numerical models of atmosphere and ocean that are trying to forecast the meteotsunamigenic disturbances and meteotsunamis, (iii) algorithms able to detect potential events, and (iv) stochastic surrogate forecasting of hazard in the most affected places. The example of the operational system in the Adriatic Sea, which unfortunately has not been running for some time due to the unavailability of super-computing resources, is displayed in Figure 28.

Aside the development of operational meteotsunamis systems, a great effort has been recently developed in researching different aspects of meteotsunamis that might be of great use for future development of early warning systems, e.g., of these along the U.S. coastlines (Angove et al., 2020). That includes all aspects of meteotsunamis, from measuring and modelling of their source in the atmosphere, through generation and spreading of meteotsunami waves, their coastal impact, hazard assessment, climatology, until operational services and early warning systems. For that purpose, the special issue of the journal Natural Hazards entitled “Science of meteorological tsunamis: a global perspective” has being undergoing with a great collection of papers already published at the journal’s webpage at https://link.springer.com/journal/11069/online-first

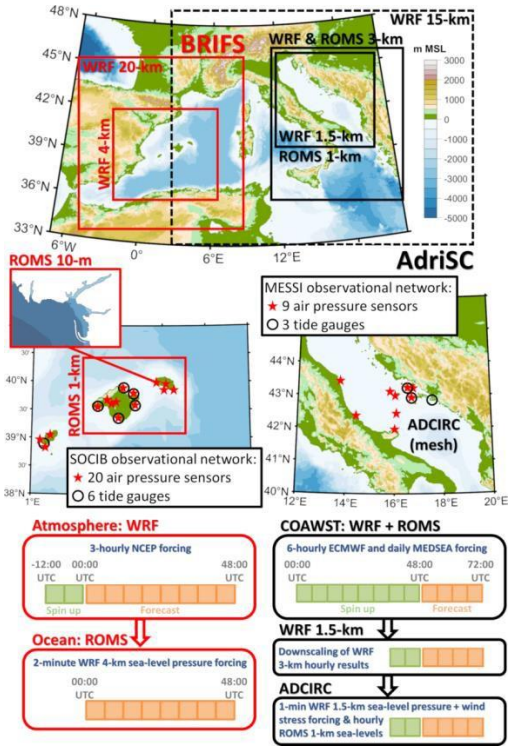

Figure 27 : Existing meteotsunami monitoring and forecasting systems in the Mediterranean Sea: BRIFS (in red) associated with the SOCIB observational network in the Balearic Islands and AdriSC forecast system (in black) associated with the MESSI observational network in the Adriatic Sea (after Vilibić et al., 2020).

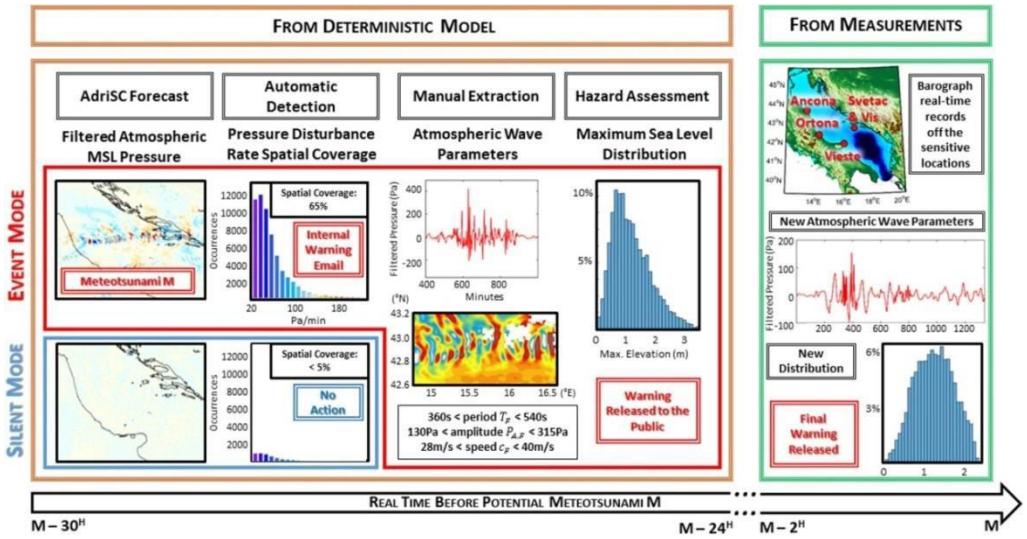

Figure 28 :. Operational meteotsunami hazard forecast within the Croatian Meteotsunami Early Warning System, based on atmospheric pressure field input from both (1) the deterministic model results (brown box) and (2) the measurements (green box). Every day, at least 30 h before any meteotsunami event, the highpass filtered pressure is extracted from the AdriSC forecast and used to automatically detect meteotsunamis by checking the spatial coverage of the values above 20 Pa per 4-min interval of the maximal pressure temporal rate. If this coverage is below 5%, then no meteotsunami is forecasted (blue box)—"silent" warning mode, otherwise a potential meteotsunami M is foreseen to occur (red box)—"event" warning mode, and an email is sent to the AdriSC team. At least 24 h before the potential meteotsunami M occurs, the first forecast of hazard assessment is derived from the stochastic surrogate model used with ranges of pressure wave parameters manually extracted from the modelled filtered pressure. Finally, when the real-time observations become available, the hazard assessment is updated with new parameters extracted from the measurements (after Denamiel et al. 2019b).

4 REFERENCES

Chapter 1

Alasset Pierre-Jean, Hélène Hébert, Said Maouche, Valérie Calbini, Mustapha Meghraoui, The tsunami induced by the 2003 Zemmouri earthquake (MW= 6.9, Algeria): modelling and results, Geophysical Journal International, Volume 166, Issue 1, July 2006, Pages 213–226, https://doi.org/10.1111/j.1365-246X.2006.02912.x

Basili, R., Brizuela, B., Herrero, A., Iqbal, S., Lorito, S., Maesano, F. E., et al. (2018). NEAM Tsunami Hazard Model 2018 (NEAMTHM18): online data of the Probabilistic Tsunami Hazard Model for the NEAM Region from the TSUMAPS-NEAM project. Istituto Nazionale di Geofisica e Vulcanologia (INGV) Available at: http://doi.org/10.13127/tsunami/neamthm18 [Accessed June 6, 2020].

Basili, R., Brizuela, B., Herrero, A., Iqbal, S., Lorito, S., Maesano, F. E., et al. (2019). NEAMTHM18 Documentation: the making of the TSUMAPS-NEAM Tsunami Hazard Model 2018. Zenodo doi:10.5281/zenodo.3406625.

Basili, R. et al. The making of the NEAM Tsunami Hazard Model 2018 (NEAMTHM18). Front. Earth Sci. 8, 616594 https://doi.org/10.3389/feart.2020.616594 (2021)

Behrens, J. et al. Probabilistic tsunami hazard and risk analysis—a review of research gaps. Front. Earth Sci. 9, 628772, https://doi.org/10.3389/feart.2021.628772 (2021).

Bernardi, F., Lomax, A., Michelini, A., Lauciani, V., Piatanesi, A., and Lorito, S. (2015). Appraising the Early-est earthquake monitoring system for tsunami alerting at the Italian Candidate Tsunami Service Provider. Nat. Hazards Earth Syst. Sci. 15, 2019–2036. doi:https://doi.org/10.5194/nhess-15-2019-2015.

Dipartimento della Protezione Civile (2018). Indicazioni alle Componenti ed alle Strutture operative del Servizio nazionale di protezione civile per l'aggiornamento delle pianificazioni di protezione civile per il rischio maremoto - Normativa. Dipartimento Della Prot. Civ. Available at: http://www.protezionecivile.gov.it/amministrazione-trasparente/provvedimenti/dettaglio/-/asset_publisher/default/content/indicazioni-alle-componenti-ed-alle-strutture-operative-del-servizio-nazionale-di-protezione-civile-per-l-aggiornamento-delle-pianificazioni-di-prot-1 [Accessed September 15, 2020].

Dziewonski, A. M., T.-A. Chou and J. H. Woodhouse, Determination of earthquake source parameters from waveform data for studies of global and regional seismicity, J. Geophys. Res., 86, 2825-2852, 1981. doi:10.1029/JB086iB04p02825

Ekström, G., M. Nettles, and A. M. Dziewonski, The global CMT project 2004-2010: Centroid-moment tensors for 13,017 earthquakes, Phys. Earth Planet. Inter., 200-201, 1-9, 2012. doi:10.1016/j.pepi.2012.04.002

Favalli, M., Boschi, E., Mazzarini, F., and Pareschi, M. T. (2009). Seismic and landslide source of the 1908 Straits of Messina tsunami (Sicily, Italy). Geophys. Res. Lett. 36. doi:10.1029/2009GL039135.

Field, E. H., Arrowsmith, R., Biasi, G. P., Bird, P., Dawson, T. E., Felzer, K. R., et al. (2014). Uniform California Earthquake Rupture Forecast, version 3 (UCERF3) -The time-independent model. Bull. Seismol. Soc. Am. 104, 1122–1180. doi:10.1785/0120130164.

Field, E. H., Jordan, T. H., Page, M. T., Milner, K. R., Shaw, B. E., Dawson, T. E., et al. (2017). A Synoptic View of the Third Uniform California Earthquake Rupture Forecast (UCERF3). Seismol. Res. Lett. 88, 1259– 1267. doi:10.1785/0220170045.

Fraser, S. A.; Power, W. L. (2013). Validation of a GIS-based attenuation rule for indicative tsunami evacuation zone mapping. GNS Science Report 2013/02 21 p.

Grezio, A., Babeyko, A., Baptista, M. A., Behrens, J., Costa, A., Davies, G., et al. (2017). Probabilistic Tsunami Hazard Analysis: Multiple Sources and Global Applications. Rev. Geophys. 55, 1158–1198. doi:10.1002/2017RG000579.

Guidoboni, E., Ferrari, G., Tarabusi, G., Sgattoni, G., Comastri, A., Mariotti, D., et al. (2019). CFTI5Med, the new release of the catalogue of strong earthquakes in Italy and in the Mediterranean area. Sci. Data 6, 80. doi:10.1038/s41597-019-0091-9.

Hayes, G., 2018, Slab2 - A Comprehensive Subduction Zone Geometry Model: U.S. Geological Survey data release, https://doi.org/10.5066/F7PV6JNV.

Leonard, G., Power, W., Lukovic, B., Smith, W., Johnston, D., and Downes, G. (2008). Interim tsunami evacuation planning zone boundary mapping for the Wellington and Horizons regions defined by a GIS-calculated attenuation rule. Lower Hutt, N.Z.: GNS Science.

Løvholt, F., Lorito, S., Macias, J., Volpe, M., Selva, J., and Gibbons, S. (2019). Urgent Tsunami Computing. in 2019 IEEE/ACM HPC for Urgent Decision Making (UrgentHPC) (Denver, CO, USA: IEEE), 45–50. doi:10.1109/UrgentHPC49580.2019.00011.

Løvholt, F., Glimsdal, S., and Harbitz, C. B. (2020). On the landslide tsunami uncertainty and hazard. Landslides. doi:10.1007/s10346-020-01429-z.

Lopez-Venegas, A. M., ten Brink, U. S., & Geist, E. L. (2008). Submarine landslide as the source for the October 11, 1918 Mona Passage tsunami: Observations and modeling. Marine Geology, 254(1-2), 35-46.

Maramai, A., Brizuela, B., and Graziani, L. (2014). The Euro-Mediterranean Tsunami Catalogue. Ann. Geophys. 57, 0435. doi:10.4401/ag-6437.

Mohamed Hamdache, José A. Peláez, A. Karim Yelles-Chauche; The Algiers, Algeria Earthquake (Mw 6. 8) of 21 May 2003: Preliminary Report. Seismological Research Letters ; 75 (3): 360–367. doi: https://doi.org/10.1785/gssrl.75.3.360

Molinari, I., Tonini, R., Lorito, S., Piatanesi, A., Romano, F., Melini, D., et al. (2016). Fast evaluation of tsunami scenarios: uncertainty assessment for a Mediterranean Sea database. Nat. Hazards Earth Syst. Sci. 16, 2593–2602. doi:https://doi.org/10.5194/nhess-16-2593-2016.

National Geophysical Data Center / World Data Service (NGDC/WDS). 2017. Global Historical Tsunami Database. NOAA. doi:10.7289/V5PN93H7 (access date).

New Zealand, and Ministry of Civil Defence & Emergency Management (2008). Tsunami evacuation zones: director's guideline for Civil Defence Emergency Management Groups. Wellington, N.Z.: Ministry of Civil Defence & Emergency Management Available at: http://www.mcdem.govt.nz/memwebsite.nsf/Files/Director_Guidelines/$file/tsunami-evacuation-zones-web.pdf [Accessed July 22, 2020].

New Zealand, and Ministry of Civil Defence & Emergency Management (2016). Tsunami evacuation zones: director's guideline for Civil Defence Emergency Management Groups. Wellington, N.Z.: Ministry of Civil Defence & Emergency Management.

Rosas, F. M., Duarte, J. C., Schellart, W. P., Tomás, R., & Terrinha, P. (2016). Seismic Potential of Thrust- Wrench Tectonic Interference between Major Active Faults Offshore SW Iberia. Geophysical Monograph Series, (210), 193-217. https://doi.org/10.1002/9781119054146.ch9

Santos, R., Caldeira, B., Bezzeghoud, M. et al. The Rupture Process and Location of the 2003 Zemmouri–Boumerdes Earthquake (Mw 6.8) Inferred from Seismic and Geodetic Data. Pure Appl. Geophys. 172, 2421–2434 (2015). https://doi.org/10.1007/s00024-014-0978-5

Selva, J., Tonini, R., Molinari, I., Tiberti, M. M., Romano, F., Grezio, A., et al. (2016). Quantification of source uncertainties in Seismic Probabilistic Tsunami Hazard Analysis (SPTHA). Geophys. J. Int. 205, 1780– 1803. doi:10.1093/gji/ggw107.

Selva, J., Lorito, S., Perfetti, P., Tonini, R., Romano, F., Piatanesi, A., et al. (2019). Probabilistic Tsunami Forecasting (PTF) for Tsunami Early Warning operations. in Geophysical Research Abstracts (Vienna), EGU2019-17775, solicited presentation, 2019.

Selva, J., Amato, A., Armigliato, A., Basili R., Bernardi F., Brizuela B., Cerminara M., de' Micheli Vitturi M., Di Bucci D., Di Manna P., Esposti Ongaro T., Lacanna G., Lorito S., Løvholt F., Mangione D., Panunzi E., Piatanesi A., Ricciardi A., Ripepe M., Romano F., Santini M., Scalzo A., Tonini R., Volpe M., Zaniboni F. (2021a). Tsunami risk management for crustal earthquakes and non-seismic sources in Italy. Riv. Nuovo Cim. 44, 69–144. https://doi.org/10.1007/s40766-021-00016-9

Selva, J., Lorito, S., Volpe, M., Romano F., Tonini R., Perfetti P., Bernardi F., Taroni M., Scala A., Babeyko A., Løvholt F., Gibbons S.J., Macías J., Castro M.J., González-Vida J.M., Sánchez-Linares C., Bayraktar H.B., Basili R., Maesano F.E., Tiberti M.M., Mele F., Piatanesi A., Amato A. (2021b). Probabilistic tsunami forecasting for early warning. Nat Commun 12, 5677. https://doi.org/10.1038/s41467-021-25815-w

Tonini R, Di Manna P, Lorito S, Selva J, Volpe M, Romano F, Basili R, Brizuela B, Castro MJ, de la Asunción M, Di Bucci D, Dolce M, Garcia A, Gibbons SJ, Glimsdal S, González-Vida JM, Løvholt F, Macías J, Piatanesi A, Pizzimenti L, Sánchez-Linares C and Vittori E (2021) Testing Tsunami Inundation Maps for Evacuation Planning in Italy. Front. Earth Sci. 9:628061. doi: 10.3389/feart.2021.628061

Woessner, J., Laurentiu, D., Giardini, D., Crowley, H., Cotton, F., Grünthal, G., et al. (2015). The 2013 European Seismic Hazard Model: key components and results. Bull. Earthq. Eng. 13, 3553–3596. doi:10.1007/s10518-015-9795-1.

Zahibo, N., Pelinovsky, E., Yalciner, A., Kurkin, A., Koselkov, A., & Zaitsev, A. (2003). The 1867 Virgin Island tsunami: observations and modeling. Oceanologica Acta, 26(5-6), 609-621.

Chapter 2.11 – 2.31 – 2.41

Bertolaso G, De Bernardinis B, Bosi V, Bosi V, Cardaci C, Ciolli S, Colozza R, Cristiani C, Mangione D, Ricciardi A, Rosi M, Scalzo A, Soddu P (2009) Civil protection preparedness and response to the 2007 eruptive crisis of Stromboli volcano, Italy. Journal of Volcanology and Geothermal Research 182: 269–277.

Chiocci, F. L., Romagnoli, C., Tommasi, P., and Bosman, A. (2008). The Stromboli 2002 tsunamigenic submarine slide: Characteristics and possible failure mechanisms. J. Geophys. Res. 113, B10102. doi:10.1029/2007JB005172.

Dipartimento della Protezione Civile, and Regione Sicilia (2015). Isola di Stromboli - Piano nazionale di emergenza a fronte di eventi vulcanici di rilevanza nazionale. Available at: http://www.protezionecivile.gov.it/resources/cms/documents/Piano_nazionale_Stromboli_2015.pdf#?R;68001?# [Accessed September 22, 2020].

Di Traglia, F., Nolesini, T., Intrieri, E., Mugnai, F., Leva, D., Rosi, M., et al. (2014). Review of ten years of volcano deformations recorded by the ground-based InSAR monitoring system at Stromboli volcano: a tool to mitigate volcano flank dynamics and intense volcanic activity. Earth-Sci. Rev. 139, 317–335. doi:10.1016/j.earscirev.2014.09.011.

Fernández-Nieto, E. D., Bouchut, F., Bresch, D., Castro Díaz, M. J., and Mangeney, A. (2008). A new Savage–Hutter type model for submarine avalanches and generated tsunami. J. Comput. Phys. 227, 7720–7754. doi:10.1016/j.jcp.2008.04.039.

Fernández-Nieto, E. D., Parisot, M., Penel, Y., and Sainte-Marie, J. (2018). A hierarchy of dispersive layer-averaged approximations of Euler equations for free surface flows. Commun. Math. Sci. 16, 1169–1202. doi:10.4310/CMS.2018.v16.n5.a1.

Fornaciai, A., Favalli, M., and Nannipieri, L. (2019). Numerical simulation of the tsunamis generated by the Sciara del Fuoco landslides (Stromboli Island, Italy). Sci. Rep. 9, 18542. doi:10.1038/s41598-019-54949-7.

Giudicepietro, F., López, C., Macedonio, G., Alparone, S., Bianco, F., Calvari, S., et al. (2020). Geophysical precursors of the July-August 2019 paroxysmal eruptive phase and their implications for Stromboli volcano (Italy) monitoring. Sci. Rep. 10, 10296. doi:10.1038/s41598-020-67220-1.

Lacanna, E., and Ripepe, M. (2020). Genesis of tsunami waves generated by Pyroclastic flows and the Early-Warning system. in Session S13. The summer 2019 Stromboli paroxysms: a precious opportunity to expand the knowledge on the volcano. (Catania, Italy).

Løvholt, F., Pedersen, G., Harbitz, C. B., Glimsdal, S., and Kim, J. (2015). On the characteristics of landslide tsunamis. Philos. Trans. R. Soc. Math. Phys. Eng. Sci. 373, 20140376. doi:10.1098/rsta.2014.0376.

Lovholt, F., Lorito, S., Macias, J., Volpe, M., Selva, J., and Gibbons, S. (2019b). Urgent Tsunami Computing. in 2019 IEEE/ACM HPC for Urgent Decision Making (UrgentHPC) (Denver, CO, USA: IEEE), 45–50. doi:10.1109/UrgentHPC49580.2019.00011.

Ma, G., Shi, F., and Kirby, J. T. (2012). Shock-capturing non-hydrostatic model for fully dispersive surface wave processes. Ocean Model. 43–44, 22–35. doi:10.1016/j.ocemod.2011.12.002.

Macías, J., Vázquez, J. T., Fernández-Salas, L. M., González-Vida, J. M., Bárcenas, P., Castro, M. J., et al. (2015). The Al-Borani submarine landslide and associated tsunami. A modelling approach. Mar. Geol. 361, 79–95. doi:10.1016/j.margeo.2014.12.006.

Macias J, de la Asuncion M (2019) Faster and faster tsunami simulations with ChEESE. AGU Fall Meeting Abstracts 33.

Maramai, A., Graziani, L., Alessio, G., Burrato, P., Colini, L., Cucci, L., et al. (2005). Near- and far-field survey report of the 30 December 2002 Stromboli (Southern Italy) tsunami. Mar. Geol. 215, 93–106. doi:10.1016/j.margeo.2004.11.009.

Maramai, A., Brizuela, B., and Graziani, L. (2014). The Euro-Mediterranean Tsunami Catalogue. Ann. Geophys. 57, 0435. doi:10.4401/ag-6437

Marchetti E, Genco R, Ripepe M (2009) Ground deformation and seismicity related to the propagation and drainage of the dyke feeding system during the 2007 effusive eruption at Stromboli volcano (Italy). J Volcanol Geotherm Res 182(3-4):155-161. doi:10.1016/j.jvolgeores.2008.11.016

Pistolesi M, Delle Donne D, Pioli L, Rosi M, Ripepe M (2011) The 15 March 2007 explosive crisis at Stromboli Volcano, Italy: assessing physical parameters through a multidisciplinary approach. J Geophys Res 116:B12206. doi:10.1029/2011JB008527

Ripepe M., Lacanna G., Pistolesi M., Silengo M.C., Aiuppa A., Laiolo M., Massimetti F., Innocenti L., Della Schiava M., Bitetto M., La Monica F.P., Nishimura T., Rosi M., Mangione D., Ricciardi A., Genco R., Coppola D., Marchetti E., Delle Donne D. (2021), Ground deformation reveals the scale-invariant conduit dynamics driving explosive basaltic eruptions. Nature Comm. (in press)

Ripepe M, Delle Donne D, Genco R, Maggio G, Pistolesi M, Marchetti E, Lacanna G, Ulivieri G, Poggi P (2015) Volcano seismicity and ground deformation unveil the gravity-driven magma discharge dynamics of a volcanic eruption. Nat. Commun 6:6998. doi:10.1038/ncomms7998

Ripepe M, Delle Donne D, Lacanna G, Marchetti E, Ulivieri G (2009) The onset of the 2007 Stromboli effusive eruption recorded by an integrated geophysical network. J Volcanol Geotherm Res 182(3-4):131-136. doi:10.1016/j.jvolgeores.2009.02.011

Tinti S, Manucci A, Pagnoni G, Armigliato A. (2005) The 30 December 2002 landslide-induced tsunamis in Stromboli: sequence of the events reconstructed from the eyewitness accounts. Nat Hazards Earth Syst Sci 5: 763–775, doi: 10.5194/nhess-5-763-2005

Tinti, S., Maramai, A., Armigliato, A., Graziani, L., Manucci, A., Pagnoni, G., et al. (2006a). Observations of physical effects from tsunamis of December 30, 2002 at Stromboli volcano, southern Italy. Bull. Volcanol. 68, 450–461. doi:10.1007/s00445-005-0021-x.

Tinti, S., Pagnoni, G., and Zaniboni, F. (2006b). The landslides and tsunamis of the 30th of December 2002 in Stromboli analysed through numerical simulations. Bull. Volcanol. 68, 462–479. doi:10.1007/s00445-005-0022-9

Valade, S., Lacanna, G., Coppola, D., Laiolo, M., Pistolesi, M., Delle Donne, D., Genco, R., Marchetti, E., Ulivieri, G., Allocca, C., Cigolini, C., Nishimura, T., Poggi, P., Ripepe, M. (2016). Tracking dynamics of magma migration in open-conduit systems. Bull Volcanol 78, 78. https://doi.org/10.1007/s00445-016-1072-x

Chapter 2.12

Walter T. H., M. Haghighi, F. M. Schneider, D. Coppola, M. Motagh, J. Saul, A. Babeyko, T. Dahm, V. R. Troll, F. Tilmann, S. Heimann, S. Valade, R. Triyono, R. Khomarudin, N. Kartadinata, M. Laiolo, F. Massimetti and P. Gaebler (2019) Complex hazard cascade culminating in the Anak Krakatau sector collapse, nature communications,https://www.nature.com/articles/s41467-019-12284-5

Chapter 2.14 – 2.44

https://www.aknes.no/lastned.asp?_page=dokument&_id=8678&_subid=4496

https://www.aknes.no/aknes3/data/4497.pdf

Chapter 2.2

Abadie, S., Harris, J.C., Grilli, S., Fabre, R., 2012. Numerical modeling of tsunami waves generated by the flank collapse of the Cumbre Vieja Volcano (La Palma, Canary Islands): Tsunami source and near field effects. Journal of Geophysical Research 117, C05030.

Begét, J.E., 2000. Volcanic tsunamis. In: Sigurdsson, H., Houghton, B., Mc Nutt, S.R., Rymer, H., Stix, J. Encyplopedia of Volcanoes. Academic Press, 1005-1013.

Bougouin, A., Paris, R., Roche, O., 2020. Impact of fluidized granular flows into water: implications for tsunamis

generated by pyroclastic flows. Journal of Geophysical Research, Solid Earth 125, e2019JB018954.

Cas, R.A.F., Wright, J.V., 1991. Subaqueous pyroclastic flows and ignimbrites: an assessment. Bulletin of Volcanology 53, 357-380.

Carey, S., Sigurdsson, H., Mandeville, C., Bronto, S., 2000. Volcanic hazards from pyroclastic flow discharge into the sea: examples from the 1883 eruption of Krakatau, Indonesia. Geological Society of America Special Papers 345, 1-14.

de Lange, W.P., Prasetya, G.S., Healy, T.R., 2001. Modelling of tsunamis generated by pyroclastic flows (ignimbrites). Natural Hazards 24, 251-266.

Esposti Ongaro T, de' Michieli Vitturi M, Cerminara M, Fornaciai A, Nannipieri L, Favalli M, Calusi B, Macías J, Castro MJ, Ortega S, González-Vida JM and Escalante C (2021) Modeling Tsunamis Generated by Submarine Landslides at Stromboli Volcano (Aeolian Islands, Italy): A Numerical Benchmark Study. Front. Earth Sci. 9:628652. doi: 10.3389/feart.2021.628652

Freundt, A., 2003. Entrance of hot pyroclastic flows into the sea: experimental observations. Bulletin of Volcanology 65, 144-164.

Fritz, H., Hager, W., Minor, H., 2004. Near Field Characteristics of Landslide Generated Impulse Waves. Journal of Waterway Port Coastal and Ocean Engineering 130, 287-302.

Giachetti, T., Paris, R., Kelfoun, K., Ontowirjo, B., 2012. Tsunami hazard related to a flank collapse of Anak Krakatau volcano, Sunda Strait, Indonesia. Geological Society, London, Special Publication 361, 79-89.

Goto, A., Taniguchi, H., Yoshida, M., Ohba, T., Oshima, H., 2001. Effects of explosion energy and depth to the formation of blast wave and crater: field explosion experiment for the understanding of volcanic explosion. Geophysical Research Letters 28, 4287-4290.

Gray, J.P., Monaghan, J.J., 2003. Caldera collapse and the generation of waves. Geochemistry, Geophysics, Geosystems 4(2), 1015.

Grilli, S. T., Watts, P., 2005. Tsunami generation by submarine mass failure. In: Modeling, Experimental Validation, and Sensitivity Analyses. Journal of Waterway, Port, Coastal, and Ocean Engineering 131, 283–297.

Grilli, S.T., Tappin, D.R., Carey, S., Watt, S.F.L., Ward, S.N., Grilli, A.R., Engwell, S.L., Zhang, C., Kirby, J.T., Schambach, L., Muin, M., 2019. Modelling of the tsunami from the December 22, 2018 lateral collapse of Anak Krakatau volcano in the Sunda Straits, Indonesia. Scientific Reports (2019) 9, 11946.

Harbitz, C.B., 1992. Model simulations of tsunamis generated by the Storregga slide. Marine Geology 105, 1-21.

Harbitz, C.B., Løvholt, F., Pedersen, G., Masson, D.G., 2006. Mechanisms of tsunami generation by submarine landslides: a short review. Norw. J. Geol. 86, 255–264.

Heidarzadeh, M., Satake, K., 2017. A Combined Earthquake–Landslide Source Model for the Tsunami from the 27 November 1945 Mw 8.1 Makran Earthquake. Bulletin of the Seismological Society of America 107, 1033-1040.

Heller, V., Hager, W.H., 2010. Impulse product parameter in landslide generated impulse waves. The Journal of Waterway, Port, Coastal, and Ocean Engineering 136, 145–155.

Heller, V., Hager, W. H., 2011. Wave types of landslide generated impulse waves. Ocean Engineering 38, 630–640.

Heller, V., Hager, W. H., 2014. A universal parameter to predict subaerial landslide tsunamis? Journal of Marine Science and Engineering 2, 400-412.

Heller, V., Spinneken, J., 2015. On the effect of the water body geometry on landslide–tsunamis: Physical insight from laboratory tests and 2D to 3D wave parameter transformation. Coastal Engineering Journal 104, 113–134.

Heinrich, P., 1992. Nonlinear water waves generated by submarine and aerial landslides. Journal of Waterway, Port, Coastal, and Ocean Engineering 118, 249-266.

Iglesias, O., Lastras, G., Canals, M., Olabarrieta, M., González, M., Aniel-Quiroga, I., Otero, L., Durán, R., Amblas, D., Casamor, J.L., Tahchi, E., Tinti, S., De Mol, B., 2012. The BIG'95 Submarine Landslide– Generated Tsunami: A Numerical Simulation. The Journal of Geology 120, 31-48.

Imamura, F., Hashi, K., Imteaz, M. A., 2001. Modeling for tsunamis generated by landsliding and debris flow. In:

Hebenstreit G.T. (eds) Tsunami Research at the End of a Critical Decade. Advances in Natural and Technological Hazards Research 18. Springer, Dordrecht, 209–228.

Kedrinskii, V.K., 2005. Hydrodynamics of Explosion. Springer, Berlin, Heidelberg, 362 p.

Kelfoun, K., Giachetti, T., Labazuy, P., 2010. Landslide-generated tsunamis at Reunion Island. Journal of Geophysical Research 115, F04012.

Le Méhauté, B.L., 1971. Theory of explosion-generated water waves, in: Advances in Hydroscience, vol. 7, edited by: Chow, V. T., Academic Press, New York, London, 1–79.

Le Méhauté, B.L., Wang, S., 1996. Water waves generated by underwater explosion. Advanced Series on Ocean Engineering 10, World Scientific Publishing, New Jersey, 384 p.

Lee, C.H., Huang, Z., 2020. Multi-phase flow simulation of impulsive waves generated by a sub-aerial granular landslide on an erodible slope. Landslides, s10346-020-01527-y.

Løvholt, F., Pedersen, G, Harbitz, C.B., Glimsdal, S., Kim, J., 2015. On the characteristics of landslide tsunamis. Philosophical Transactions of the Royal Society A 373, 20140376.

Ma, K.F., Kanamori, H., Satake, K., 1999. Mechanism of the 1975 Kalapana, Hawaii, earthquake inferred from tsunami data. Journal of Geophysical Research 104 B6, 13,153-13,167.

Ma, G., Shi, F. and Kirby, J. T., 2012. Shock-capturing non-hydrostatic model for fully dispersive surface wave processes. Ocean Modelling,43-44, 22-35.

Mader, C. L., 2002. Modeling the 1958 Lituya Bay mega tsunami, Ⅱ. Science of Tsunami Hazards 20, 241-250.

Maeno, F., Imamura, F., 2011. Tsunami generation by a rapid entrance of pyroclastic flow into the sea during the 1883 Krakatau eruption, Indonesia. Journal of Geophysical Research 116, B09205.

Maeno, F., Imamura, F., Taniguchi, H., 2006. Numerical simulations of tsunamis generated by caldera collapse during the 7.3 ka Kikai eruption, Kyushu, Japan. Earth Planets Space 58, 1013-1024.

Mirchina, N. R., Pelinovsky, E. N., 1988. Estimation of underwater eruption energy based on tsunami wave data, Nat. Hazards 1, 277–283.

Mohammed, F., & Fritz, H. M. (2012). Physical modeling of tsunamis generated by three-dimensional deformable granular landslides. Journal of Geophysical Research, 117, C11015.

Nomanbhoy, N., Satake, K., 1995. Generation mechanism of tsunamis from the 1883 Krakatau eruption. Geophysical Research Letters 22(4), 509-512.

Paris, A., Heinrich, P., Paris, R., Abadie, S., 2020. The December 22, 2018 Anak Krakatau, Indonesia, landslide and tsunami: preliminary modeling and results. Pure and Applied Geophysics 177, 571–590.

Paris, R., 2015. Source mechanisms of volcanic tsunamis. Philosophical Transactions of the Royal Society A 373, 20140380.

Paris, R., Switzer, A.D., Belousova, M., Belousov, A., Ontowirjo, B., Whelley, P.L., Ulvrová, M., 2014. Volcanic tsunami: a review of source mechanisms, past events and hazards in Southeast Asia (Indonesia, Philippines, Papua New Guinea). Natural Hazards 70 (1), 447-470.

Paris, R., Ulvrova, M., Selva, J., Brizuela, B., Costa, A., Grezio, A., Lorito, S., Tonini, R., 2019. Probabilistic hazard analysis for tsunamis generated by subaqueous volcanic explosions in the Campi Flegrei caldera, Italy. Journal of Volcanology and Geothermal Research 379, 106-116.

Paris, R., Ulvrova, M., 2019. Tsunamis generated by subaqueous volcanic explosions in Taal Caldera Lake, Philippines. Bulletin of Volcanology 81, 14.

Roche, O., Phillips, J.C., Kelfoun, K., 2013. Pyroclastic density currents. In: Fagents et al. (Eds.), mldeling volcanic processes: the physics and mathematics of volcanism. Cambridge University Press.

Satake, K., Kato, Y., 2001. The 1741 Oshima-Oshima eruption: extent and volume of submarine debris avalanche. Geophysical Research Letters 28, 427-430.

Satake, K., 2012. Tsunamis generated by submarine landslides. Submarine mass mocements and their consequences, Springer, pp. 475-484.

Sato, H., Taniguchi, H., 1997. Relationship between crater size and ejecta volume of recent magmatic and phreato-

magmatic eruptions: implications for energy partitioning, Geophys. Res. Lett. 24, 205–208.

Selva, J., Amato, A., Armigliato, A. et al (2021a). Tsunami risk management for crustal earthquakes and non-seismic sources in Italy. Riv. Nuovo Cim. 44, 69–144. https://doi.org/10.1007/s40766-021-00016-9

Tehranirad, B., Harris, J.C., Grilli, A.R., Grilli, S.T., Abadie, S., Kirby, J.T., Shi, F., 2015. Far-field tsunami threat in the north Atlantic basin from large scale flank collapses of the Cumbre Vieja volcano, La Palma. Pure and Applied Geophysics 172, 3589-3616.

Tinti, S., Pagnoni, G., Zaniboni, F., 2006. The landslides and tsunamis of the 30th of December 2002 in Stromboli analysed through numerical simulations. Bulletin of Volcanology. 68, 462–479.

Torsvik, T., Paris, R., Didenkulova, I., Pelinovsky, E., Belousov, A., Belousova, M., 2010. Numerical simulation of a tsunami event during the 1996 volcanic eruption in Karymskoye lake, Kamchatka, Russia, Nat. Hazards Earth Syst. Sci. 10, 2359–2369.

Ulvrova, M., Paris, R., Kelfoun, K., Nomikou, P., 2014. Numerical simulations of tsunami generated by underwater volcanic explosions at Karymskoye Lake (Kamchatka, Russia) and Kolumbo volcano (Aegean Sea, Greece). Natural Hazards and Earth System Sciences 14, 401-412.

Ulvrova, M., Paris, R., Nomikou, P., Kelfoun, K., Leibrandt, S., Tappin, D.R., McCoy, F.W., 2016. Source of the tsunami generated by the 1650 AD eruption of Kolumbo submarine volcano (Aegean Sea, Greece). Journal of Volcanology and Geothermal Research 321, 125-139.

Vacondio, R., Mignosa, P., Pagani, S., 2013. 3d SPH numerical simulation of the wave generated by the Vajont rockslide. Advances in Water Resources 59, 146-156.

Viroulet, S., Cébron, D., Kimmoun, O., & Kharif, C. (2013). Shallow water waves generated by subaerial solid landslides. Geophysical Journal International, 193, 747–762.

Wang X, Mountjoy JJ, Power WL, Lane EM, Mueller C (2016) Revealing the failure process of a submarine landslide near Cook Strait and its associated tsunami. Submarine mass movements and their consequences, Springer, pp. 599-606.

Ward, S.N., 2001. Landslide tsunami. Journal of Geophysical Research 6, 11201-11215.

Watts, P., 1998. Wavemaker curves for tsunamis generated by underwater landslides. Journal of Waterway, Port, Coastal, and Ocean Engineering 124, 127-137.

Watts, P., Waythomas, C.F., 2003. Theoretical analysis of tsunami generation by pyroclastic flows. Journal of Geophysical Research 108B112, 2563.

Watts, P., Grilli, S.T., Kirby, J.T., Fryer, G.J., Tappin, D.R., (2003). Landslide tsunami case studies using Boussinesq model and a fully nonlinear tsunami generation model. Nat. Haz. Earth Sys. Sci. 3: 391-402.

Xenakis, A. M., Lind, S. J., Stansby, P. K., Rogers B. D., 2017. Landslides and tsunamis predicted by incompressible smoothed particle hydrodynamics (SPH) with application to the 1958 Lituya Bay event and idealized experiment. Proceedings of the Royal Society A 473, 20160674.

Yavari-Ramshe S., Ataie-Ashtiani B., 2016. Numerical modeling of subaerial and submarine landslide-generated tsunami waves - recent advances and future challenges. Landslides 13(6), 1325-1368.

Zhao, T., Utili, S., Crosta, G.B., 2016. Rockslide and impulse wave modelling of the Vajont reservoir by DEM-CFD analyses. Rock Mechanics and Rock Engineering 49, 2437-2456.

ANNEX1 (Table)

Blong, R.J., McKee, C.O., 1995. The Rabaul eruption 1994 - Destruction of a town. Natural Hazards Research Center, Macquarie University, Australia, 52 p.

Froger, J.L., Famin, V., Cayol, V., Augier, A., Michon, L., Lénat, J.F., 2015. Time-dependent displacements during and after the April 2007 eruption of Piton de la Fournaise, revealed by interferometric data. Journal of Volcanology and Geothermal Research 296, 55-68.

Maramai, A., Graziani, L., Tinti, S., 2005. Tsunamis in the Aeolian Islands Southern Italy: a review. Marine Geology 214, 11-21.

Paris, A., Heinrich, P., Paris, R., Abadie, S., 2020. The December 22, 2018 Anak Krakatau, Indonesia, landslide and tsunami: preliminary modeling and results. Pure and Applied Geophysics 177, 571–590.

Paris, R., Ulvrova, M., 2019. Tsunamis generated by subaqueous volcanic explosions in Taal Caldera Lake, Philippines. Bulletin of Volcanology 81, 14.

Paris, R., Switzer, A.D., Belousova, M., Belousov, A., Ontowirjo, B., Whelley, P.L., Ulvrová, M., 2014. Volcanic tsunami: a review of source mechanisms, past events and hazards in Southeast Asia Indonesia, Philippines, Papua New Guinea. Natural Hazards 70, 447-470.

Pelinovsky, E., Zahibo, N., Dunkley, P., Edmonds, M., Herd, R., Talipova, T., Kozelkov, A., Nikolkina I., 2004. Tsunamis generated by the volcano eruption on July 12-13, 2003 at Montserrat, Lesser Antilles. Science of Tsunami Hazards 22, 44-57.

Simkin, T., Fiske, R.S., 1983. Krakatau 1883: The volcanic eruption and its effects. Smithsonian Institution Press, Washington DC, 464 p.

Chapter 2.32

Giachetti, T., Paris, R., Kelfoun, K., Ontowirjo, B., 2012. Tsunami hazard related to a flank collapse of Anak Krakatau volcano, Sunda Strait, Indonesia. Geological Society, London, Special Publication 361, 79-89.

Paris, R., Switzer, A.D., Belousova, M., Belousov, A., Ontowirjo, B., Whelley, P.L., Ulvrová, M., 2014. Volcanic tsunami: a review of source mechanisms, past events and hazards in Southeast Asia (Indonesia, Philippines, Papua New Guinea). Natural Hazards 70 (1), 447-470.

Chapter 2.33

Dahl-Jensen, T., Larsen, L. M., Pedersen, S. A. S., Pedersen, J.,Jepsen, H. F., Pedersen, G., et al. (2004). Landslide and Tsunami 21 November 2000 in Paatuut, West Greenland. Natural Hazards, 31(1), 277–287.

NOAA. (2018). National Geophysical Data Center/ World Data Service: NCEI/WDS Global Historical Tsunami Database. NOAA National Centers for Environmental Information. https://data.nodc.noaa.gov/cgi-bin/iso?id=gov.noaa.ngdc.mgg.hazards: G02151

Paris A, Okal EA, Guérin C, Heinrich P, Schindelé F, Hébert H (2019) Numerical modeling of the June 17, 2017 landslide and Tsunami events in Karrat Fjord, West Greenland. Pure appl Geophys 176(7):3035–3057. https ://doi.org/10.1007/s0002 4-019-02123 -5

Chapter 2.42

Chapters 2.13 and 2.43

Kato T, Terada Y, Tadokoro K, Kinugasa N, Futamura A, Toyoshima M, Yamamoto S, Ishii M, Tsugawa T, Nishioka M, Takizaka K, Shoji Y, Seka H (2018) Development of GNSS buoy for a synthetic geohazard monitoring system. J Disaster Res 13(3):460–471. https ://doi.org/10.20965 /jdr.2018.p0460

Ozaki T (2012) JMA's Tsunami warning for the 2011 Great Tohoku earthquake and Tsunami improvement plan. J Disaster Res 7:439–445. https ://doi.org/10.20965 /jdr.2012.p0439

NOWPHAS, Nationwide Ocean Wave information network for Ports and HArbourS. https://www.mlit.go.jp/kowan/nowphas/index_eng.html.

S-net and DONET, Nationwide observation network for earthquakes, tsunamis, and volcanoes over land and sea https://www.mowlas.bosai.go.jp/mowlas/?LANG=en

Kamigaichi O. (2015) Tsunami Forecasting and Warning, Encyclopedia of Complexity and Systems Science, DOI10.1007/978-3-642-27737-5_568-3

Chapter 2.45

Chapter 3

Angove, M., Kozlosky, L., Chu, P., Dusek, G., Mann, G., Anderson, E.J., Gridley, J., Arcas, D., Titov, V., Eble, M., McMahon, K., Hirsch, B., Zaleski, W., 2020. Addressing the meteotsunami risk in the United States. Natural Hazards, under review.

Denamiel, C., Šepić, J., Ivanković, D., Vilibić, I., 2019a. The Adriatic Sea and coast modelling suite: Evaluation of the meteotsunami forecast component. Ocean Modelling, 135, 71-93.

Denamiel, C., Šepić, J., Huan, X., Bolzer, C., Vilibić, I., 2019b. Stochastic surrogate model for meteotsunami early warning system in the eastern Adriatic Sea. Journal of Geophysical Research Oceans, 124, 8485-8499.

Monserrat, S., Vilibić, I., Rabinovich, A.B., 2006. Meteotsunamis: atmospherically induced destructive ocean waves in the tsunami frequency band. Natural Hazards and Earth System Sciences, 6, 1035-1051

Rabinovich AB (2020) Twenty-seven years of progress in the science of meteorological tsunamis following the 1992 Daytona Beach event. Pure and Applied Geophysics, 177, 1193–1230.

Renault, L., Vizoso, G., Jansà, A., Wilkin, J., & Tintoré, J. (2011). Toward the predictability of meteotsunamis in the Balearic Sea using regional nested atmosphere and ocean models. Geophysical Research Letters, 38, L10601. https://doi.org/10.1029/2011gl047361.

Vilibić, I., Denamiel, C., Zemunik, P., Denamiel, C., 2020. The Mediterranean and Black Sea meteotsunamis: An overview. Natural Hazards, https://doi.org/10.1007/s11069-020-04306-z.

ANNEX 1 :

List of potentially tsunamigenic volcanoes in the world. Modified and updated from Paris et al. (2014) for South-East Asia, and the National Geophysical Data Center / World Data Service (NCEI/WDS Global Historical Tsunami Database. NOAA National Centers for Environmental Information).

NAME	COUNTRY	VOLCANO TYPE	DISTANCE / COAST (km)	LAST ERUPTION	HISTORICAL TSUNAMI
Kadovar	PAPUA - NEW GUINEA	A	0.5	2020	2018
Kilauea	HAWAII, USA	D	14	2020	1975
Kavachi	SOLOMON ISLANDS	C	0	2020	1951
Stromboli	AEOLIAN ISLANDS, ITALY	A	1.6	2020	1916, 1919, 1930, 1944, 1954, 2002, 2019
Tinakula	SOLOMON ISLANDS	A	1.1	2020	1897, 1966
Anak Krakatau	SUNDA STRAIT, INDONESIA	B	0.5	2020	1883, 1928, 1930, 1981, 2018
Taal	LUZON, PHILIPPINES	B	2.2	2020	1716, 1749, 1754, 1911, 1965
Barren Island	ANDAMA ISLANDS, INDIA	A	1.5	2020	
Sangeang Api	FLORES SEA, INDONESIA	A	5.2	2020	
Karangetang	SULAWESI, INDONESIA	A	4	2020	
Suwanose-jima	RYUKYU ISLANDS, JAPAN	A	2.2	2020	
Manam	PAPUA - NEW GUINEA	A	5	2020	
Nishino-jima	IZU ISLANDS, JAPAN	B	0.2	2020	
Kikai	RYUKYU ISLANDS, JAPAN	B	1	2020	
Yasur	TANNA ISLAND, VANUATU	B	2.2	2020	
Piton de la Fournaise	REUNION ISLAND, FRANCE	D	9	2020	
White Island	NEW ZEALAND	A	0.8	2019	
Raikoke	KURIL ISLANDS, RUSSIA	A	0.7	2019	
Lateiki	TONGA	C	0	2019	
Kick’em Jenny	GRENADA	C	0	2017	1939, 1965?
Unnamed	TONGA	C	0	2017	
Momotombo	NICARAGUA	A	3.5	2016	
Hunga	TONGA	B	0.1	2015	
Tofua	TONGA	A	3	2014	1892

Rabaul	PAPUA - NEW GUINEA	B	0.6	2014	1878, 1937, 1994
Soufriere Hills	MONTSERRAT	A	3.2	2013	1997, 1999, 2003, 2006
Iliwerung	LEMBATA, INDONESIA	A	1.5	2013	1973, 1979, 1983
Paluweh Island	FLORES SEA, INDONESIA	A	2.3	2013	1928
Batu Tara	FLORES SEA, INDONESIA	A	1	2013	
Lewotolo	LEMBATA, INDONESIA	A	4	2012	
South Sarigan	MARIANA ISLANDS, USA	C	0	2010	2010
NW-Rota 1	MARIANA ISLANDS, USA	C	0	2010	
Miyake-jima	IZU ISLANDS, JAPAN	A	3	2010	
Anatahan	MARIANA ISLANDS, USA	A	1.5	2008	
Ritter Island	PAPUA - NEW GUINEA	C	0	2007	1888, 1972, 1974, 2007
Lopevi	VANUATU	A	2.2	2007	
Augustine	ALASKA, USA	A	4	2006	1883
Home Reef	TONGA	C	0	2006	
Awu	SULAWESI, INDONESIA	A	5.5	2004	1856, 1892
Ruang	SULAWESI, INDONESIA	A	1.6	2002	1871
Tori-jima	IZU ISLANDS, JAPAN	A	1.1	2002	
Ruby	MARIANA ISLANDS, USA	C	0	1995	
Banda Api	BANDA SEA, INDONESIA	A	1.5	1988	
Didicas	PHILIPPINES	B	0.2	1978	1969?
Bam	PAPUA - NEW GUINEA	A	1.1	1960	
Camiguin	BOHOL SEA, PHILIPPINES	B	4	1953	1871
Vulcano	AEOLIAN ISLANDS, ITALY	B	0.9	1890	1988
Cosiguina	NICARAGUA	A	6.1	1859	1835?
Oshima-Oshima	JAPAN SEA, JAPAN	A	1	1790	1741
Kolumbo	AEGEAN SEA, GREECE	C	0	1650	1650

This table is a list of volcanoes that are currently potentially tsunamigenic, following the criteria defined by Paris et al. (2014). We have added the following criteria as filters: (1) the volcano must be located less than 1000 km from populated areas; (2) the volcano has been active during the XXth or XXIst centuries (except for four of them). We have also mentioned if the volcano was a validated source of tsunami during the four last centuries.

As proposed by Paris et al. (2014), an active or dormant volcano is considered to be potentially tsunamigenic if it belongs to one of the following types of volcanoes:

A- It is a steep-flanked stratovolcano whose main eruptive centre is located less than 6 km from the coast (sea or lake). In such cases the main tsunamigenic mechanisms are pyroclastic flows and flank instability, from rock falls (10^6 m³) to debris avalanches (10^8 to 10^9 m³). The typical example is Stromboli volcano (Aeolian Islands, Italy), whose activity and recurrent flank instability generated 7 tsunamis since the year 1900 (Maramai et al., 2005). Another example case-study was provided by the 1995-2010 eruption of Soufrière Hills, during which 4 tsunamis were generated by the entrance of pyroclastic flows into the sea (Pelinovsky et al., 2004).

B- The volcano belongs to a complex of eruptive centres in a partly submerged caldera. A distinction can be made between caldera lakes (e.g. Taal, Philippines, 5 tsunamis since AD 1700: Paris & Ulvrova, 2019), calderas opened to the sea (e.g. Rabaul, Papua-New Guinea, tsunamis in 1878, 1937 and 1994: Blong & McKee, 1995) and submerged calderas with emerged eruptive centres (e.g. Anak Krakatau, Indonesia, tsunamis associated with the major 1883 eruption, and more recently in 2018: Simkin & Fiske, 1983; Paris et al., 2020). Potential tsunami sources in such volcanic systems include pyroclastic flows, underwater explosions, rapid ground subsidence (e.g., caldera collapse), and small-scale flank instability.

C- It is a submarine volcano, whose activity (e.g., underwater explosions at shallow depth) and instability (e.g., submarine landslide, collapse of newly formed lava bench) are clearly potential sources of tsunamis. Sites of interest here include Kick'em Jenny volcano in the Caribbean, and Ritter Island in the Bismarck Sea.

D- It is a shield volcano (ocean island) showing evidence of flank deformation, such as Kilauea volcano in Hawaii (e.g., Kalapana earthquake and tsunami in 1975: Ma et al., 1999), and Piton de la Fournaise in Reunion Island (e.g., lar-scale flank deformation observed during the 2007 eruption: Froger et al., 2015).